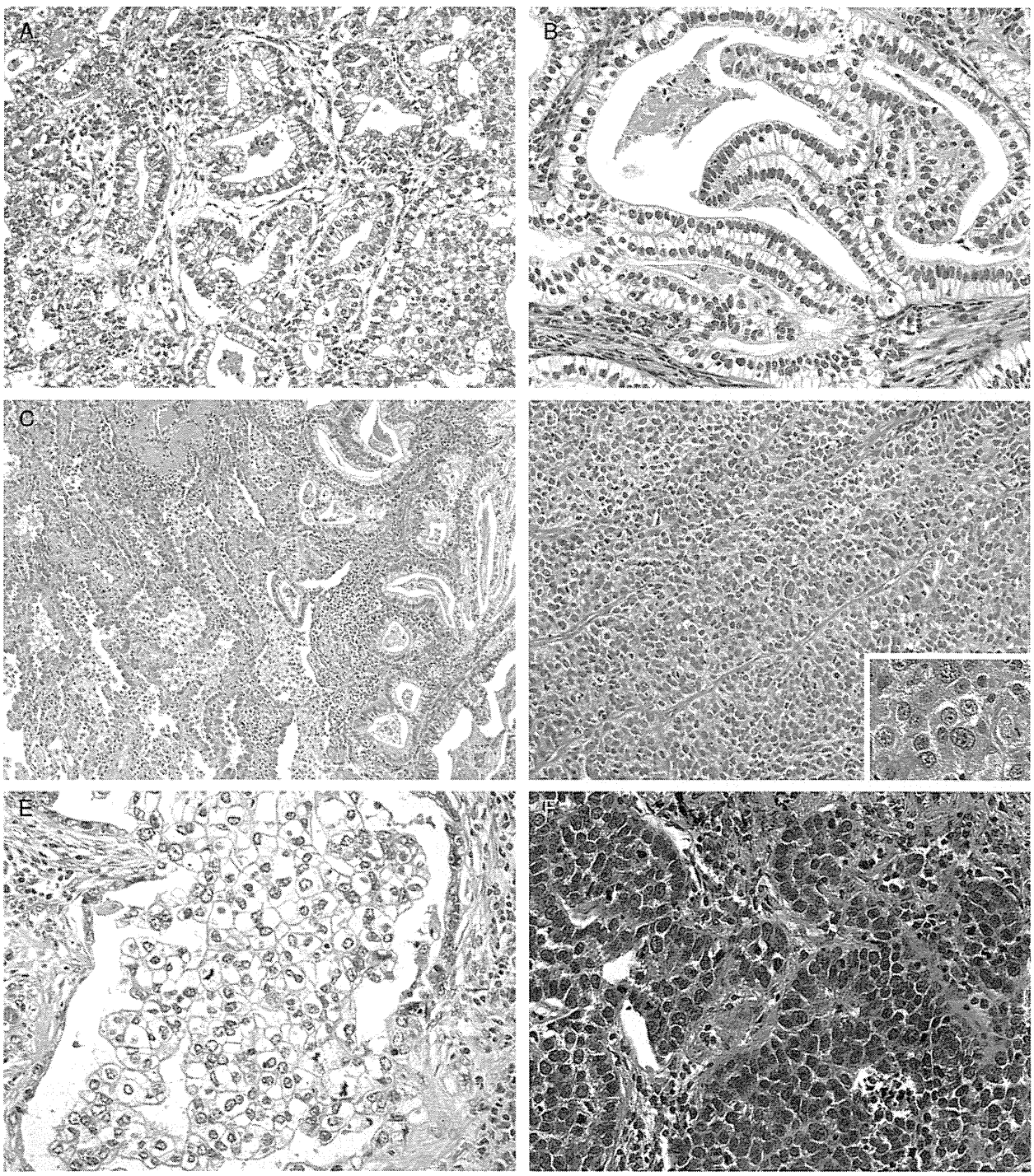

FIGURE 1. HG-LAFM showed at least focal element that resembles developing fetal lung (A and B), in which columnar cells with supranuclear or subnuclear cytoplasmic clearing displayed complex glandular architecture. Fetal lung–like component was invariably accompanied by conventional adenocarcinoma (C, right: fetal lung–like pattern; left: conventional pattern). Hepatoid (D, inset shows a magnified view of hepatoid cells) and clear-cell patterns (E) were overrepresented in non–fetal lung–like component. HG-LAFM was combined with LCNEC in 4 cases (F).

HG-LAFMs predominantly occurred in old men with a consistent heavy smoking history, unlike low-grade carcinoma, which develops in younger patients with a female predominance.[5,8,10,21] Second, a fetal lung–like component in HG-LAFMs was invariably a focal finding accompanied by a histology that did not resemble that of a

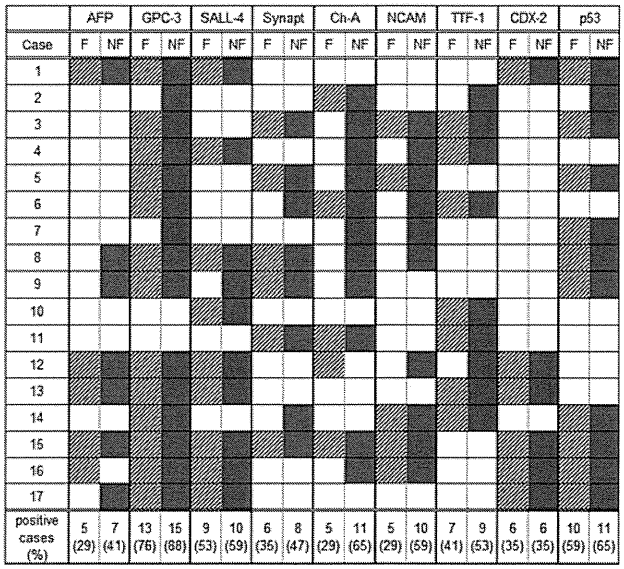

FIGURE 2. Immunoprofiles of 17 HG-LAFMs. The left halves of the 2 boxes for each molecule show the results in fetal lung–like component. The right halves show the result in the coexisting non–fetal lung–like component. A filled box represents positive staining. An empty box means a negative result. F denotes a fetal lung–like component; NF, a non–fetal lung–like component; Synapt, synaptophysin; Ch-A, chromogranin A; NCAM, neural cell adhesion molecule; TTF-1, thyroid transcription factor-1.

fetal lung, whereas low-grade adenocarcinoma of the fetal lung type was reported to manifest typically in a pure fetal lung–like form.[10,11,21] Third, all of our HG-LAFMs lacked morule formation and aberrant immunoexpression of β-catenin, which are 2 signature findings of low-grade adenocarcinoma of the fetal lung type.[10,11] We therefore agree with Nakatani et al[8] that low-grade and high-grade lung adenocarcinomas harboring fetal lung–like morphology are completely different diseases, rather than 2 related tumors in the same family differing only in their grades. In this respect, we believe that the current WHO classification system is somewhat confusing because both low-grade and high-grade tumors are read under the same heading by the name of well-differentiated and poorly differentiated fetal adenocarcinoma, respectively. From a practical standpoint, careful wording is necessary when discussing fetal lung–like morphology in a report of high-grade tumors in order to avoid confusion with low-grade adenocarcinoma. We elected to use HG-LAFM terminology in this report because of the concern that the originally proposed "high-grade adenocarcinoma of fetal lung type"[8] terminology might give an inaccurate impression of its relatedness with low-grade adenocarcinoma of fetal lung type.

Coexisting non–fetal lung–like histology in HG-LAFM was quite heterogenous, and it included all 4 common growth patterns of conventional adenocarcinoma: lepidic, papillary, acinar, and solid patterns. Nonetheless, our data suggest that fetal lung–like differentiation has a peculiar tendency to admix with particular non–fetal lung–like morphologic attributes. Specifically, hepatoid morphology and clear-cell pattern, 2 uncommon phenotypes in lung adenocarcinoma,[14–18] appeared to be overrepresented in the non–fetal lung–like component. These results suggest that fetal lung–like morphology might not be a mere capricious phenotypic variation that any given lung cancer might display, but it might represent a line of differentiation that only a particular subset of lung cancer can undergo.

In agreement with a previous study,[8] we showed that as many as approximately 80% of HG-LAFMs displayed immunohistochemical evidence of neuroendocrine differentiation. Although immunoreactivity to neuroendocrine markers can be seen in 16% to 36% of morphologically nondescript lung adenocarcinomas,[22–24] the rate of positivity appeared high in HG-LAFMs, which suggests a clearer tendency of neuroendocrine differentiation in this tumor subset. Supporting this hypothesis, 4 of 17 HG-LAFMs in our series displayed morphologic evidence of neuroendocrine differentiation in the form of admixture with LCNEC. In no report of the relevant literature has HG-LAFM with LCNEC component been clearly described, although 1 putative example of HG-LAFM[6] was reportedly associated with "carcinoid-like neuroendocrine component," and the latter element might meet the contemporary criteria of LCNEC.

An increased level of serum AFP was identified in 4 of 5 cases tested. Immunohistochemical AFP staining was demonstrated in 8 cases (47%). This observation is consistent with those of a previous study[8] in which 29% of HG-LAFM demonstrated AFP immunoexpression. AFP production in adenocarcinoma was reported in many other organ systems, and it has been documented most commonly in stomach cancers. AFP-producing stomach cancer is known to occur in elderly patients, and it is characterized by prominent vascular invasion and frequent liver metastasis.[25–28] Previous histologic analyses of AFP-producing gastric carcinoma have identified several characteristic morphologic patterns: primitive gut (enteroblastic), hepatoid, clear-cell, and yolk sac tumor like.[26–30] It is particularly interesting that the histology of primitive gut–type (enteroblastic) stomach cancer was described and illustrated as having a complex glandular structure lined by columnar cells with clear cytoplasm.[26–28,30] To a great degree, its morphology overlaps fetal lung–like histology that we describe in lung cancer (compare our Figs. 1A and B with the histology of AFP-producing stomach cancers depicted in Image 2 of Maitra et al,[26] Figure 2 of Kodama et al,[27] Figure 4 of Motoyama et al,[28] and Figure 1 of Matsunou et al[30]). Nakatani et al,[8] in their original series, also recognized this resemblance.

The histologic analogy between lung and stomach cancers is strengthened further by the frequent coexistence of hepatoid and clear-cell patterns in our HG-LAFMs, because these 2 patterns are also common in AFP-producing stomach cancers.[26–32] Immunohistochemical analysis provided yet another support for this parallel, in that

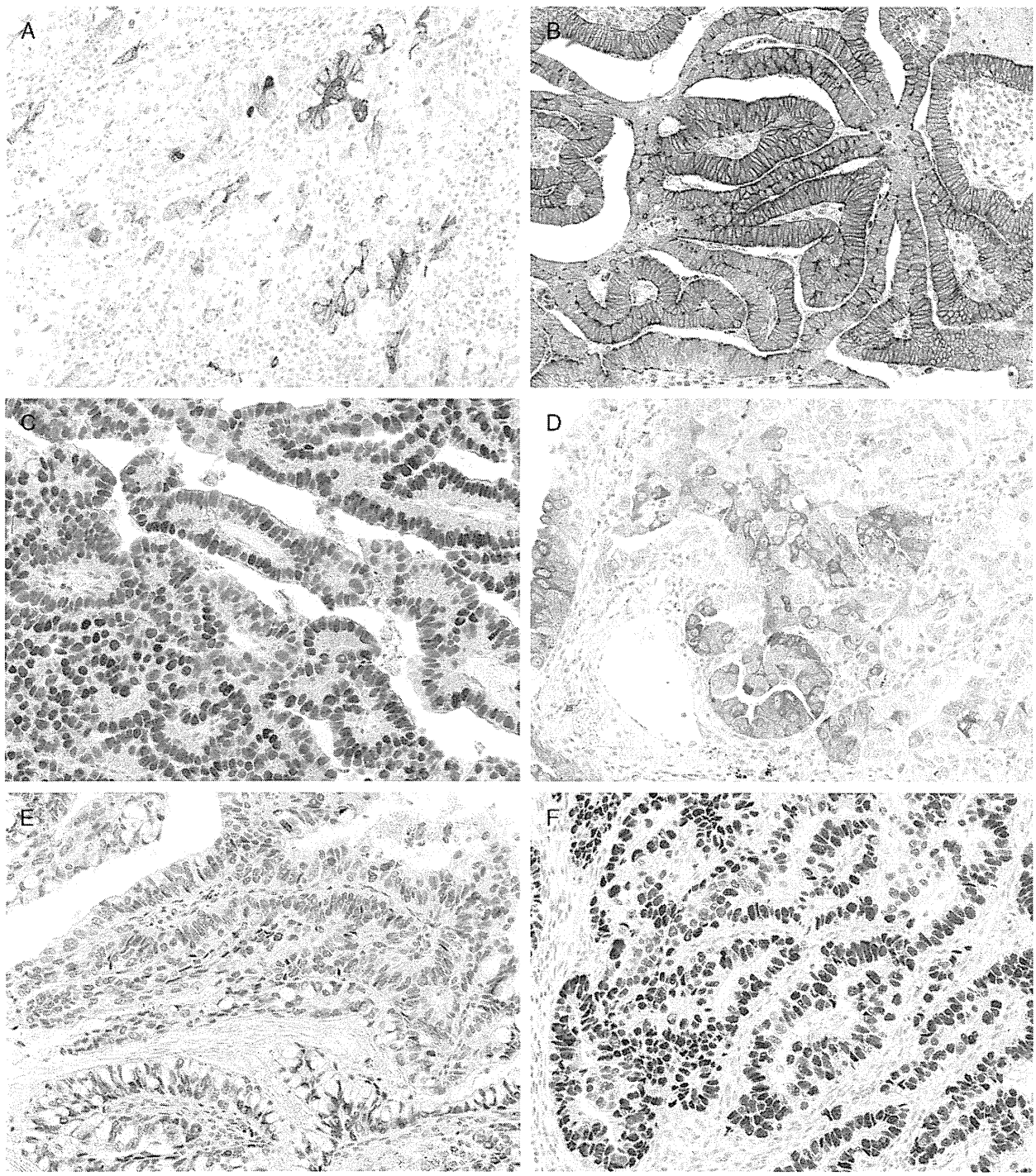

FIGURE 3. Immunohistochemical staining of HG-LAFM. AFP staining was observed in a subset of cases (A). HG-LAFM frequently showed membranous and cytoplasmic staining for GPC-3 (B) and nuclear staining for SALL-4 (C). Neuroendocrine markers were positive in most cases (D, synaptophysin staining). Some tumors were positive for CDX-2 (E) and p53 (F).

GPC-3 and SALL-4, 2 sensitive markers of AFP-producing stomach cancer,[29,31,32] are often expressed in HG-LAFMs. The lung and stomach are both developed from the foregut, and AFP-producing stomach cancer and HG-LAFM (which might also produce AFP) might be regarded as showing similar oncofetal retrograde differentiation in terms of its morphology and immunoprofile. Intestinal marker CDX-2 expression, identified in 35% of our HG-LAFMs, might further suggest a close link between fetal lung–like histology in lung cancer and

TABLE 4. Molecular Characteristics of 17 High-grade Lung Adenocarcinomas With Fetal Lung–like Morphology

Case	*EGFR* Mutation	*KRAS* Mutation
1	WT	WT
2	L858R	WT
3	WT	WT
4	WT	WT
5	WT	WT
6	WT	Codon 12 or 13
7	WT	WT
8	WT	WT
9	WT	WT
10	WT	NA
11	WT	NA
12	WT	NA
13	WT	NA
14	NA	NA
15	NA	NA
16	NA	NA
17	WT	NA

NA indicates data not available; WT, wild type.

"primitive gut" differentiation in stomach cancer, because AFP-producing stomach cancers are usually of intestinal type and are positive for CDX-2.[33,34]

Results of molecular analysis suggest that HG-LAFM is not genetically homogenous. One case (7% of 14 cases tested) showed *EGFR* mutation. Another (11% of 9 cases tested) harbored *KRAS* mutation. However, it is notable that 78% of the 9 cases tested were of wild type for both *EGFR* and *KRAS*. Given the high frequency of *EGFR* and *KRAS* mutations (46% to 64% and 13%, respectively) in lung adenocarcinoma in the Japanese population,[35–37] this low rate might be worth investigation. The majority of HG-LAFMs (65%) showed positive p53 immunostaining. The rate of positivity in HG-LAFMs seems higher than that in lung adenocarcinoma in general (44% to 50%).[38,39]

In conclusion, HG-LAFM is associated with several characteristic clinicopathologic features such as male predominance, heavy smoking exposure, overrepresented coexistence with hepatoid, clear-cell, and high-grade neuroendocrine histology, and frequent immunoreactivity to neuroendocrine and oncofetal markers. Confirming the results in the original report[8] and providing additional morphologic and immunophenotypic characterization, our data indicate that HG-LAFMs might form a coherent subgroup of lung adenocarcinomas. However, the uniformly focal nature of fetal lung–like elements, widely diverse coexisting non–fetal lung–like histology, and inhomogenous molecular profiles make us hesitate to conclude that HG-LAFM truly constitutes a specific entity that is worthy of a separate entry in tumor classification. We believe that HG-LAFM is best considered for the time being as a recognizable morphologic pattern showing characteristic association with several clinicopathologic parameters. This treatment contrasts sharply with low-grade adenocarcinoma of fetal lung type, a distinct variant having homogenous fetal lung–like histology and specific genetic alteration. These 2 diseases should be confused neither in diagnostic reports nor in tumor classification. The morphologic and immunohistochemical similarity between HG-LAFM and AFP-producing stomach cancer is striking. This intriguing resemblance might open a new perspective to our understanding of HG-LAFM.

REFERENCES

1. Boyle P, Levin B. *World Cancer Report 2008*. Lyon: IARC Press, International Agency for Research on Cancer; 2008.
2. Travis WD, et al. World Health Organization, International Agency for Research on Cancer. *Pathology and Genetics of Tumours of the Lung, Pleura, Thymus, and Heart*. Lyon: IARC Press; 2004.
3. Kradin RL, Young RH, Dickersin GR, et al. Pulmonary blastoma with argyrophil cells and lacking sarcomatous features (Pulmonary endodermal tumor resembling fetal lung). *Am J Surg Pathol*. 1982;6:165–172.
4. Nakatani Y, Dickersin GR, Mark EJ. Pulmonary endodermal tumor resembling fetal lung: a clinicopathologic study of five cases with immunohistochemical and ultrastructural characterization. *Hum Pathol*. 1990;21:1097–1107.
5. Koss MN, Hochholzer L, O'Leary T. Pulmonary blastomas. *Cancer*. 1991;67:2368–2381.
6. Mardini G, Pai U, Chavez AM, et al. Endobronchial adenocarcinoma with endometrioid features and prominent neuroendocrine differentiation. A variant of fetal adenocarcinoma. *Cancer*. 1994;73:1383–1389.
7. Kodama T, Shimosato Y, Watanabe S, et al. Six cases of well-differentiated adenocarcinoma simulating fetal lung tubules in pseudoglandular stage. Comparison with pulmonary blastoma. *Am J Surg Pathol*. 1984;8:735–744.
8. Nakatani Y, Kitamura H, Inayama Y, et al. Pulmonary adenocarcinomas of the fetal lung type: a clinicopathologic study indicating differences in histology, epidemiology, and natural history of low-grade and high-grade forms. *Am J Surg Pathol*. 1998;22:399–411.
9. Nakatani Y, Miyagi Y, Takemura T, et al. Aberrant nuclear/cytoplasmic localization and gene mutation of beta-catenin in classic pulmonary blastoma - β-catenin immunostaining is useful for distinguishing between classic pulmonary blastoma and a blastomatoid variant of carcinosarcoma. *Am J Surg Pathol*. 2004;28:921–927.
10. Sekine S, Shibata T, Matsuno Y, et al. β-catenin mutations in pulmonary blastomas: association with morule formation. *J Pathol*. 2003;200:214–221.
11. Nakatani Y, Masudo K, Miyagi Y, et al. Aberrant nuclear localization and gene mutation of beta-catenin in low-grade adenocarcinoma of fetal lung type: up-regulation of the Wnt signaling pathway may be a common denominator for the development of tumors that form morules. *Mod Pathol*. 2002;15:617–624.
12. Sobin LH. Union internationale contre le cancer. *TNM Classification of Malignant Tumours*. Oxford: Wiley-Blackwell; 2009.
13. Travis WD, Brambilla E, Noguchi M, et al. International Association for the Study of Lung Cancer/American Thoracic Society/European Respiratory Society: international multidisciplinary classification of lung adenocarcinoma: executive summary. *Proc Am Thorac Soc*. 2011;8:381–385.
14. Arnould L, Drouot F, Fargeot P, et al. Hepatoid adenocarcinoma of the lung: report of a case of an unusual α-fetoprotein-producing lung tumor. *Am J Surg Pathol*. 1997;21:1113–1118.
15. Hayashi Y, Takanashi Y, Ohsawa H, et al. Hepatoid adenocarcinoma in the lung. *Lung Cancer*. 2002;38:211–214.
16. Ishikura H, Kanda M, Ito M, et al. Hepatoid adenocarcinoma: a distinctive histological subtype of alpha-fetoprotein-producing lung carcinoma. *Virchows Arch A Pathol Anat Histopathol*. 1990;417:73–80.
17. Kishimoto T, Yano T, Hiroshima K, et al. A case of α-fetoprotein-producing pulmonary carcinoma with restricted expression of

hepatocyte nuclear factor-4α in hepatoid foci: a case report with studies of previous cases. *Hum Pathol.* 2008;39:1115–1120.
18. Katzenstein ALA, Prioleau PG, Askin FB. The histologic spectrum and significance of clear-cell change in lung carcinoma. *Cancer.* 1980;45:943–947.
19. Takano T, Fukui T, Ohe Y, et al. EGFR mutations predict survival benefit from gefitinib in patients with advanced lung adenocarcinoma: a historical comparison of patients treated before and after gefitinib approval in Japan. *J Clin Oncol.* 2008;26:5589–5595.
20. Krypuy M, Newnham GM, Thomas DM, et al. High resolution melting analysis for the rapid and sensitive detection of mutations in clinical samples: KRAS codon 12 and 13 mutations in non-small cell lung cancer. *BMC Cancer.* 2006;6:295.
21. Sato S, Koike T, Yamato Y, et al. Resected well-differentiated fetal pulmonary adenocarcinoma and summary of 25 cases reported in Japan. *Jpn J Thorac Cardiovasc Surg.* 2006;54:539–542.
22. Howe M, Chapman A, Kerr K, et al. Neuroendocrine differentiation in non-small cell lung cancer and its relation to prognosis and therapy. *Histopathology.* 2005;46:195–201.
23. Ionescu DN, Treaba D, Gilks CB, et al. Nonsmall cell lung carcinoma with neuroendocrine differentiation - An entity of no clinical or prognostic significance. *Am J Surg Pathol.* 2007;31:26–32.
24. Segawa Y, Takata S, Fujii M, et al. Immunohistochemical detection of neuroendocrine differentiation in non-small-cell lung cancer and its clinical implications. *J Cancer Res Clin Oncol.* 2009;135:1055–1059.
25. Chang YC, Nagasue N, Abe S, et al. Comparison between the clinicopathologic features of AFP-positive and AFP-negative gastric cancers. *Am J Gastroenterol.* 1992;87:321–325.
26. Maitra A, Murakata LA, Albores-Saavedra J. Immunoreactivity for hepatocyte paraffin 1 antibody in hepatoid adenocarcinomas of the gastrointestinal tract. *Am J Clin Pathol.* 2001;115:689–694.
27. Kodama T, Kameya T, Hirota T, et al. Production of alpha-fetoprotein, normal serum proteins, and human chorionic gonadotropin in stomach cancer: Histologic and immunohistochemical analyses of 35 cases. *Cancer.* 1981;48:1647–1655.
28. Motoyama T, Aizawa K, Watanabe H, et al. alpha-Fetoprotein producing gastric carcinomas: a comparative study of three different subtypes. *Acta Pathol Jpn.* 1993;43:654–661.
29. Ushiku T, Uozaki H, Shinozaki A, et al. Glypican 3-expressing gastric carcinoma: distinct subgroup unifying hepatoid, clear-cell, and α-fetoprotein-producing gastric carcinomas. *Cancer Sci.* 2009;100:626–632.
30. Matsunou H, Konishi F, Jalal RE, et al. Alpha-fetoprotein-producing gastric carcinoma with enteroblastic differentiation. *Cancer.* 1994;73:534–540.
31. Ushiku T, Shinozaki A, Shibahara J, et al. SALL4 represents fetal gut differentiation of gastric cancer, and is diagnostically useful in distinguishing hepatoid gastric carcinoma from hepatocellular carcinoma. *Am J Surg Pathol.* 2010;34:533–540.
32. Hishinuma M, Ohashi K, Yamauchi N, et al. Hepatocellular oncofetal protein, glypican 3 is a sensitive marker for α-fetoprotein-producing gastric carcinoma. *Histopathology.* 2006;49:479–486.
33. Kumashiro Y, Yao T, Aishima S, et al. Hepatoid adenocarcinoma of the stomach: histogenesis and progression in association with intestinal phenotype. *Hum Pathol.* 2007;38:857–863.
34. Mizoshita T, Tsukamoto T, Nakanishi H, et al. Expression of Cdx2 and the phenotype of advanced gastric cancers: relationship with prognosis. *J Cancer Res Clin Oncol.* 2003;129:727–734.
35. Kosaka T, Yatabe Y, Onozato R, et al. Prognostic implication of EGFR, KRAS, and TP53 gene mutations in a large cohort of Japanese patients with surgically treated lung adenocarcinoma. *J Thorac Oncol.* 2009;4:22–29.
36. Mitsudomi T, Kosaka T, Endoh H, et al. Mutations of the epidermal growth factor receptor gene predict prolonged survival after gefitinib treatment in patients with non-small-cell lung cancer with postoperative recurrence. *J Clin Oncol.* 2005;23:2513–2520.
37. Haneda H, Sasaki H, Lindeman N, et al. A correlation between EGFR gene mutation status and bronchioloalveolar carcinoma features in Japanese patients with adenocarcinoma. *Jpn J Clin Oncol.* 2006;36:69–75.
38. Brambilla E, Gazzeri S, Moro D, et al. Immunohistochemical study of p53 in human lung carcinomas. *Am J Pathol.* 1993;143:199–210.
39. Tsao MS, Aviel-Ronen S, Ding K, et al. Prognostic and predictive importance of p53 and RAS for adjuvant chemotherapy in non–small-cell lung cancer. *J Clin Oncol.* 2007;25:5240–5247.

UICC
global cancer control

IJC
International Journal of Cancer

Genome structure-based screening identified epigenetically silenced microRNA associated with invasiveness in non-small-cell lung cancer

Kousuke Watanabe[1]*, Noriko Emoto[1]*, Emi Hamano[1], Mitsuhiro Sunohara[1], Masanori Kawakami[1], Hidenori Kage[1], Kentaro Kitano[2], Jun Nakajima[2], Akiteru Goto[3], Masashi Fukayama[3], Takahide Nagase[1], Yutaka Yatomi[4], Nobuya Ohishi[1] and Daiya Takai[4]

[1] Department of Respiratory Medicine, The University of Tokyo Hospital, Hongo, Bunkyo-ku, Tokyo, Japan
[2] Department of Cardiothoracic Surgery, The University of Tokyo Hospital, Hongo, Bunkyo-ku, Tokyo, Japan
[3] Department of Pathology, The University of Tokyo Hospital, Hongo, Bunkyo-ku, Tokyo, Japan
[4] Department of Clinical Laboratory, The University of Tokyo Hospital, Hongo, Bunkyo-ku, Tokyo, Japan

MicroRNA (miRNA) expression is frequently altered in human cancers. To search for epigenetically silenced miRNAs in non-small-cell lung cancer (NSCLC), we mapped human miRNAs on autosomal chromosomes and selected 55 miRNAs *in silico*. We treated six NSCLC cell lines with the DNA methylation inhibitor 5-aza-2′-deoxycytidine (5-aza-CdR) and determined the expressions of the 55 miRNAs. Fourteen miRNAs were decreased in the cancer cell lines and were induced after 5-aza-CdR treatment. After a detailed DNA methylation analysis, we found that mir-34b and mir-126 were silenced by DNA methylation. Mir-34b was silenced by the DNA methylation of its own promoter, whereas mir-126 was silenced by the DNA methylation of its host gene, *EGFL7*. A chromatin immunoprecipitation assay revealed H3K9me2 and H3K9me3 in mir-34b and *EGFL7*, and H3K27me3 in *EGFL7*. The overexpression of mir-34b and mir-126 decreased the expression of c-Met and Crk, respectively. The 5-aza-CdR treatment of lung cancer cell line resulted in increased mir-34b expression and decreased c-Met protein. We next analyzed the DNA methylation status of these miRNAs using 99 primary NSCLCs. Mir-34b and mir-126 were methylated in 41 and 7% of all the cases, respectively. The DNA methylation of mir-34b was not associated with c-Met expression determined by immunohistochemistry, but both mir-34b methylation ($p = 0.007$) and c-Met expression ($p = 0.005$) were significantly associated with lymphatic invasion in a multivariate analysis. The DNA methylation of mir-34b can be used as a biomarker for an invasive phenotype of lung cancer.

Cancer Genetics

MicroRNAs (miRNAs) are broadly conserved small non-coding RNA that regulate gene expression by binding to the 3′UTR of target mRNAs in a complementary manner.[1] Through the posttranscriptional regulation of many target genes, miRNAs are involved in many biological processes, such as development and human carcinogenesis. MicroRNA expression is altered in human cancers, and some miRNAs have oncogenic or tumor suppressive functions in human malignancies, including lung cancer.[2–5]

Key words: microRNA, DNA methylation, lung cancer
Additional Supporting Information may be found in the online version of this article.
*K.W. and N.E. contributed equally to the work.
Grant sponsor: Smoking Research Foundations, Takeda Science Foundation and KAKENHI; **Grant numbers:** 20659129, 22790749
DOI: 10.1002/ijc.26254
History: Received 7 Feb 2011; Accepted 1 Jun 2011; Online 23 Jun 2011
Correspondence to: Daiya Takai, M.D., PhD., Department of Clinical Laboratory, The University of Tokyo Hospital, 7-3-1, Hongo, Bunkyo-ku, Tokyo 113-8655, Japan, Tel.: +81-3-3815-5411 (extension 37725), Fax: +81 3 5689 0495, E-mail: dtakai-ind@umin.ac.jp

Chromosomal deletions or amplifications are important mechanisms of miRNA expression change in cancers. For example, mir-15 and mir-16 are frequently deleted and downregulated in chronic lymphocytic leukemia.[2] The mir-17-92 miRNA cluster is amplified and overexpressed in B-cell lymphoma[6] and lung cancer.[4] However, the precise mechanisms responsible for changes in miRNA expression in cancer remain largely unknown.

DNA methylation plays an important role in inactivating tumor suppressor genes in many types of human cancers.[7,8] Recently, DNA methylation in cancerous tissue has been shown to cause the silencing of miRNAs located in the vicinity of CpG islands.[9,10] As the epigenetic silencing of tumor suppressor genes is a common event in lung carcinogenesis[11–14] and miRNA expression is altered in lung cancer,[5] we decided to search for epigenetically silenced miRNAs in lung cancer.

In our study, we selected 55 candidate miRNAs *in silico* based on the genome structure and treated six non-small-cell lung cancer (NSCLC) cell lines with the DNA methylation inhibitor 5-aza-2′-deoxycytidine (5-aza-CdR). Among the suppressed miRNAs whose expressions were induced by 5-aza-CdR, we found that mir-34b and mir-126 were silenced

by DNA methylation. Mir-126 was silenced by the DNA methylation of its host gene, *EGFL7*. We then analyzed the histone modifications and the suppression of target genes by the overexpression of the miRNAs. We also determined the DNA methylation status of 99 primary NSCLCs and found that miRNA methylation was associated with histological invasiveness.

Material and Methods

Cell lines and 5-aza-CdR treatment

H1755, H2347, H1650, H1975, Calu-1, A549 and HEK293t were obtained from the American Type Culture Collection. LC1sq was obtained from the Health Science Research Resources Bank (Osaka, Japan). Normal human bronchial epithelial cell (NHBE) was obtained from Lonza (Basel, Switzerland). These cell lines were cultured according to each manufacturer's protocol. Genomic DNA was extracted using the standard proteinase K/phenol method,[15] and the total RNA was isolated using RNAiso (Takara, Shiga, Japan).

Six NSCLC cell lines (H1755, H2347, H1650, H1975, LC1sq and Calu-1) were treated with 5-aza-CdR (Sigma-Aldrich, St. Louis, MO) on Day 1 and Day 3 for 24 hr each time (3 μM for H2347, H1650 and H1975; 5 μM for H1755, LC1sq and Calu-1). Total RNA extraction and chromatin immunoprecipitation (ChIP) analysis were performed on Day 6.

Primary NSCLC samples

We analyzed 99 primary NSCLCs from 97 histologically confirmed NSCLC patients who had undergone surgical resection at the University of Tokyo Hospital. The two patients had double primary NSCLCs, *i.e.* they had two tumors showing different pathological characteristics. To determine the miRNA expression levels in a normal control, we used normal counterpart lung tissue of each patient and also normal lung tissue from a patient with sclerosing hemangioma who underwent surgical resection at the University of Tokyo Hospital. Informed consent was obtained from all the patients, and the study was approved by the Institutional Review Board. Genomic DNA, and the total RNA were isolated as described above.

MicroRNA expression analysis

The miRNA expression levels were analyzed using quantitative reverse transcription PCR (RT-PCR) using a TaqMan microRNA assay (Applied Biosystems, Foster City, CA), in accordance with the manufacturer's instructions. U6 small nuclear RNA (RNU6B) was used as an internal control. Detailed information regarding the 55 candidate miRNAs is available in Supporting Information Table 1.

Host gene expression analysis

The total RNA was reverse transcribed with Superscript III (Invitrogen, Carlsbad, CA), and the SYBR green RT-PCR was performed using Realtime PCR Master Mix (Toyobo, Osaka, Japan). Human Spleen Total RNA (Ambion, Austin, TX) was used as a positive control for the RT-PCR of the *EGFL7* long transcript. The beta-actin gene was used as an internal control. The PCR conditions and the primer sequences are shown in Supporting Information Table 2.

DNA methylation studies

A quantitative *Hpa*II PCR assay[16] was performed to measure the methylation levels of the six cancer cell lines and NHBE. Genomic DNA was digested with *Eco*RI (New England Biolabs, Ipswich, MA) and purified using phenol/chloroform extraction; 500 ng of *Eco*RI-digested DNA were then digested with *Hpa*II or *Msp*I (New England Biolabs). The percentage of DNA that was not digested by *Hpa*II was determined using real-time PCR with THUNDERBIRD SYBR qPCR Mix (Toyobo). *Msp*I was used to confirm that the *Hpa*II-digestion was blocked by DNA methylation, and not by a genetic change.

For the bisulfite sequencing, methylation-specific PCR (MSP) and combined bisulfite restriction analysis (COBRA), 500 ng of DNA was treated with sodium bisulfite according to a previously described protocol.[11] Bisulfite PCR and MSP were performed using Amplitaq Gold 360 Master Mix (Applied Biosystems). To ensure that an equal amount of DNA was used as a template, the genomic DNA of each clinical tumor sample was digested with *Hind*III (New England Biolabs), purified using phenol/chloroform extraction and quantified using a spectrophotometer before the bisulfite conversion reaction. Fifty nanograms of bisulfite-converted DNA was used as a template for the MSP, and the methylation status was determined using agarose gel electrophoresis after 35 cycles of amplification. For COBRA, the bisulfite PCR products were treated using ExoSAP-IT (US Biochemical, Cleveland, OH), as previously described,[17] digested using *Bst*UI or *Taq*I (New England Biolabs) and visualized using agarose gel electrophoresis.

The PCR conditions and the primer sequences are shown in Supporting Information Table 2.

Chromatin immunoprecipitation assay

The ChIP analysis was performed as previously described.[18] Briefly, cells were crosslinked with 1% formaldehyde followed by sonication using a BIORUPTOR (UCD-200TM; COSMO BIO, Tokyo, Japan). The sheared chromatin was then immunoprecipitated using OneDay ChIP Kit (Diagenode, Philadelphia, PA), and the immunoprecipitated DNA was quantified using real-time PCR with THUNDERBIRD SYBR qPCR Mix (Toyobo). The antibodies used were histone H3 (tri methyl K4) antibody (ab1012; abcam, Cambridge, MA), histone H3 (di methyl K9) antibody (ab1220; abcam), histone H3 (tri methyl K9) antibody (ab8898; abcam), histone H3 (tri methyl K27) antibody (ab6002; abcam) and the negative control IgG included in the kit. The HOXA9 gene was used as a positive control for the H3K27me3 antibody, as previously

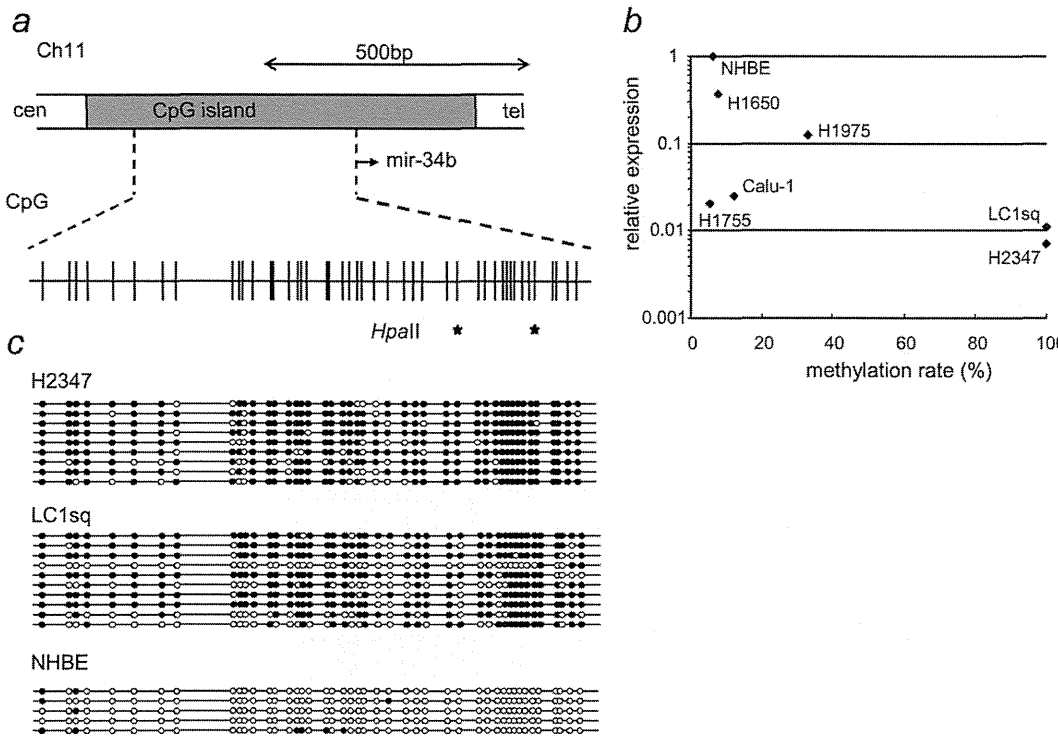

Figure 1. Epigenetic silencing of mir-34b. (*a*) Structure of mir-34b genomic locus. Mir-34b is located within a CpG island. The 5′ CpG sites and *Hpa*II sites for the DNA methylation analysis are also shown. (*b*) DNA methylation and mir-34b expression in six NSCLC cell lines and NHBE. The horizontal axis represents the DNA methylation rate determined using *Hpa*II PCR. The vertical axis represents the mir-34b expression relative to NHBE. We confirmed that more than 99% of the DNA was digested with *Msp*I in all the cell lines (data not shown), meaning that *Hpa*II digestion is blocked by DNA methylation. (*c*) Bisulfite sequencing. The open and filled circles represent unmethylated and methylated CpG sites, respectively.

described.[19,20] The PCR conditions and the primer sequences are shown in Supporting Information Table 2.

MicroRNA overexpression

The miRNA expression vector was constructed using a previously described pol III-dependent expression system.[21] The construction process is shown in Supporting Information Figure 1. Human U6 promoter containing a *Bsp*MI site was amplified using PCR with the primers U6pro-forward and U6pro-reverse-BspMI from the previously described plasmid U6pro/tetO/DNMT1,[21] then ligated into a TA cloning vector, pGEM-T Easy (Promega, Madison, WI). This plasmid was digested with *Bsp*MI (New England Biolabs), followed by the ligation of oligonucleotides (a mixture of two DNA oligomers, Oligo34bF and Oligo34bR or Oligo126F and Oligo126R) to form U6pro/mir-34b and U6pro/mir-126, respectively. A mir-126 expression cassette was triplicated to increase the expression of mature miRNA. The mir-126 expression cassette was amplified using PCR with the primers 126-forward-PstI and 126-reverse-SacI or 126-forward-SphI and 126-reverse-NcoI from U6pro/mir126, ligated into pGEM-T Easy and subcloned into the *Pst*I-*Sac*I site and *Sph*I-*Nco*I site of U6pro/mir-126. The resulting plasmid contained three miRNA expression cassettes (U6pro/mir-126*3). The mir-34b expression cassette was inverted by digestion with *Not*I (New England Biolabs). A hygromycin resistance cassette was then subcloned into the *Apa*I site from the previously described plasmid U6pro/tetO/DNMT1/hygro[21] to form U6pro/mir-34b/hygro, U6pro/mir-126*3/hygro/A and U6pro/mir-126*3/hygro/B. As a negative control, we used U6pro/Blank/hygro, which contained five Ts after the U6 promoter. The primer sequences are shown in Supporting Information Table 2.

Target gene analysis

The miRNA expression vectors and the control vector were transfected into A549 and HEK293t cells using Lipofectamine LTX reagent (Invitrogen), followed by hygromycin selection. After selection, the total protein was extracted using Radioimmunoprecipitation Assay (RIPA) buffer (phosphate buffered saline, 1% NP-40, 0.5% sodium deoxycholate, 0.1% sodium dodecyl sulfate) containing Complete Mini protease inhibitor (Roche, Basel, Switzerland), and the total RNA was isolated as described above. For the western blot analysis, 20 μg of total protein was loaded onto a 5–20% gradient

polyacrylamide gel (Wako, Osaka, Japan), electrophoresed in Tris-glycine-SDS running buffer, transferred to Hybond-P (GE Healthcare, Buckinghamshire, UK) and blotted with antibodies using the SNAP id system (Millipore, Billerica, MA). The antibodies used were c-Met antibody (1:60 dilution, sc-10; Santa Cruz Biotechnology, Santa Cruz, CA), Crk

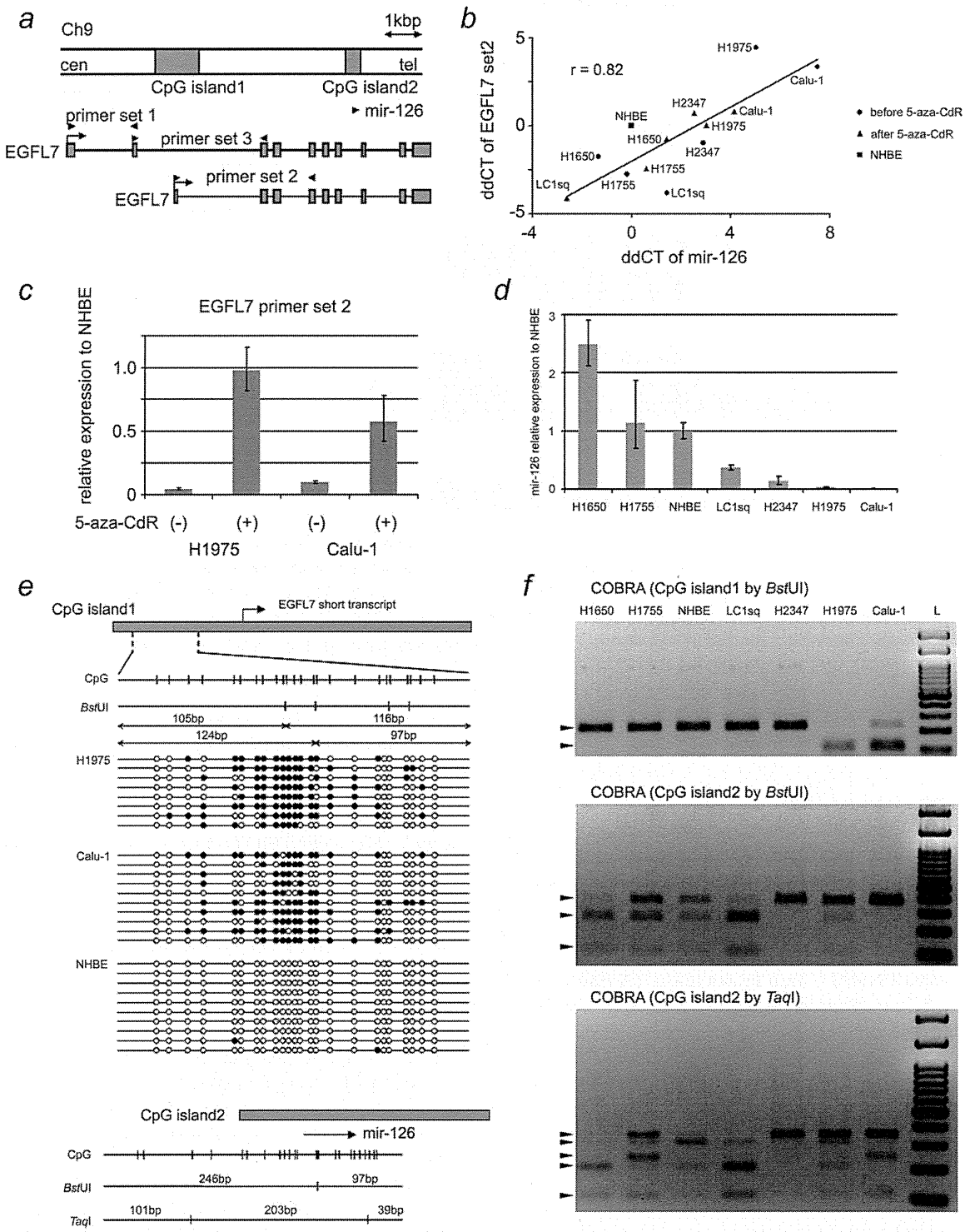

Figure 2.

II antibody (1:60 dilution, sc-9004; Santa Cruz Biotechnology), beta-actin antibody (1:3000 dilution, A5441; Sigma-Aldrich), anti-rabbit-IgG-horseradish peroxidase (HRP) antibody (1:1000 dilution for c-Met and Crk II, sc-2030; Santa Cruz Biotechnology) and anti-mouse-IgG-HRP antibody (1:2000 dilution for beta-actin, sc-2005; Santa Cruz Biotechnology). The proteins were detected using ECL plus solution (GE Healthcare) for c-Met and Crk II and ECL solution (GE Healthcare) for beta-actin. RT-PCR for c-Met and Crk was performed using THUNDERBIRD SYBR qPCR Mix (Toyobo). The PCR conditions and the primer sequences are shown in Supporting Information Table 2.

Immunohistochemistry for c-Met

A tissue microarray was constructed from formalin-fixed, paraffin-embedded tissue blocks. Immunohistochemistry was performed using antibodies against c-Met (1:100 dilution, SP44; Ventana Medical Systems, Tucson, AZ) using a Ventana Benchmark XT autostainer (Ventana Medical Systems). All the samples were evaluated by a pathologist (A.G.) who had no knowledge of any other data and were scored as previously described[22]: 0, complete absence of staining or only focal weak staining; 1, weak to moderate staining in less than 40% of the cancer cells; 2, weak to moderate staining in at least 40% of the cancer cells; and 3, strong staining in at least 10% of the cancer cells among the specimens with weak to moderate staining in at least 40% of the cancer cells. The cases were then divided into two groups: either c-Met negative (0, 1 or 2) or c-Met positive (3).

Statistical analysis

The relation between miRNA methylation, c-Met expression and clinicopathological characteristics were analyzed using chi-square test or Fisher's exact test. A logistic regression analysis was used to analyze independent factors associated with invasive phenotype. The analysis was performed using Dr.SPSS II (SPSS, Chicago, IL).

Results

Selection process of epigenetically silenced miRNAs

When our research started, the quantitative RT-PCR system using TaqMan microRNA assay (Applied Biosystems) was available for 687 miRNAs. We mapped these miRNAs on autosomal chromosomes and selected *in silico* 55 miRNAs that met one of the following criteria: (*i*) miRNAs within CpG islands, (*ii*) miRNAs within 1 kbp downstream of CpG islands and (*iii*) miRNAs within gene introns whose host promoters have CpG islands (Supporting Information Fig. 2 and Supporting Information Table 1).

After *in silico* selection, we treated six NSCLC cell lines (H1755, H2347, H1650, H1975, LC1sq and Calu-1) with 5-aza-CdR, and the expressions of the 55 miRNAs were determined (Supporting Information Fig. 3*a*). H1755 and H2347 were adenocarcinoma cell lines without epidermal growth factor receptor (EGFR) mutation; H1650 and H1975 were adenocarcinoma cell lines with EGFR mutation and LC1sq and Calu-1 were squamous cell carcinoma cell lines. The expression levels of 14 miRNAs (mir-375, mir-196b, mir-126, mir-34b, mir-127, mir-203, mir-148a, mir-181c, mir-30e, mir-449a, mir-340, mir-486, mir-483 and mir-139) were less than 25% of that in normal lung tissue and increased by more than 4-fold after 5-aza-CdR treatment. We then measured the expressions of these 14 miRNAs in 15 primary NSCLCs (Supporting Information Fig. 3*b*). Seven frequently suppressed miRNAs (mir-126, mir-34b, mir-203, mir-30e, mir-449a, mir-486 and mir-139) were selected as candidates for further analysis (Supporting Information Fig. 2).

Epigenetic silencing of mir-34b

Among the seven candidate miRNAs, three (mir-126, mir-34b and mir-203) were located within CpG islands. Mir-34b is frequently methylated in colorectal cancer,[23] and we used *Hpa*II PCR to measure the level of DNA methylation of mir-34b in the six NSCLC cell lines and NHBE cells. These cell lines showed various levels of DNA methylation (Fig. 1*b*), and mir-34b was completely methylated in the two most suppressed cell lines, H2347 and LC1sq (Figs. 1*b* and 1*c*). The treatment of these two cell lines with 5-aza-CdR resulted in an increase in mir-34b expression (Supporting Information Fig. 3*a*). These results show that mir-34b expression is regulated by DNA methylation in NSCLC. Mir-203 is also located within a CpG island, but only a low level of DNA methylation was detected using bisulfite sequencing (data not shown).

Figure 2. Epigenetic silencing of mir-126. (*a*) Structure of *EGFL7* and mi-126 genomic locus. Mir-126 is located within a CpG island and also within the intron of *EGFL7*. The locations of the primers used for the RT-PCR of *EGFL7* are also shown. (*b*) Correlation between mir-126 expression and *EGFL7* expression before (circles) and after (triangles) 5-aza-CdR treatment. The horizontal axis represents the ddCt value of mir-126 relative to NHBE. The vertical axis represents the ddCt value of *EGFL7* relative to NHBE. The linear regression line and the Pearson's correlation coefficient (*r*) are indicated. (*c*) Induction of *EGFL7* by 5-aza-CdR treatment in H1975 and Calu-1. Experiments were duplicated, and the error bars indicate the standard deviation (SD). (*d*) Mir-126 expression in six cancer cell lines (before 5-aza-CdR treatment) and NHBE. Experiments were triplicated, and the error bars indicate the SD. (*e*) Bisulfite sequencing of CpG island 1 in H1975, Calu-1, and NHBE. The CpG sites and *Bst*UI sites used for COBRA are also indicated. Open and filled circles represent unmethylated and methylated CpG sites, respectively. The CpG sites and *Bst*UI and *Taq*I sites for COBRA within CpG island 2 are shown at the bottom. (*f*) COBRA of CpG island 1 and CpG island 2 in six cancer cell lines and NHBE. The lanes are arranged in the order of mir-126 expression from left (high expression) to right (low expression). Arrowheads indicate undigested and digested DNA fragments (L, 100-bp DNA ladder).

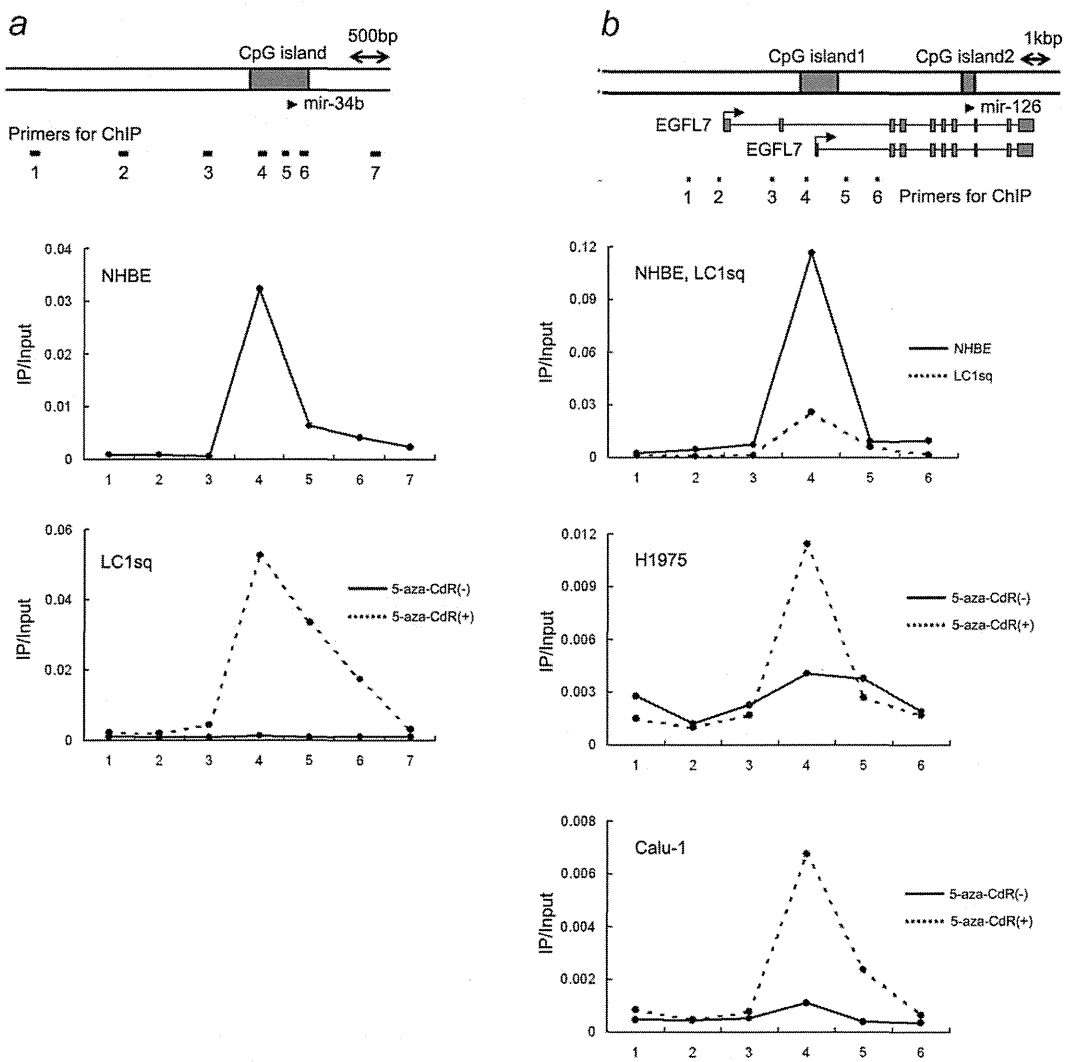

Figure 3. H3K4 trimethylation of mir-34b and mir-126. (*a*) Mapping of H3K4me3 at the mir-34b locus. The locations of the PCR primers used for ChIP are indicated. The experiments were duplicated, and the results are shown as the ratios of immunoprecipitated (IP) DNA to input DNA. (*b*) Mapping of H3K4me3 at *EGFL7* and the mir-126 locus; Otherwise as shown in Figure 3*a*.

Epigenetic silencing of mir-126 through the methylation of its host gene, EGFL7

Mir-126 is located within a CpG island and also within the intron of *EGFL7* (Fig. 2*a*). According to the UCSC Genome Bioinformatics Site (http://genome.ucsc.edu), *EGFL7* has several transcriptional variants, and one short transcript has another CpG island at its 5′ end (Fig. 2*a*).

The long *EGFL7* transcript (primer set 1, shown in Fig. 2*a*) was detected in the spleen but not in NHBE or the six NSCLC cell lines with or without 5-aza-CdR treatment (data not shown). In contrast, the short *EGFL7* transcript (primer set 2, shown in Fig. 2*a*) was detected in NHBE and the six NSCLC cell lines, and the expression of mir-126 and the short *EGFL7* transcript were strongly correlated (Pearson's correlation coefficient = 0.82, $p = 0.00048$; Fig. 2*b*). The expression of mir-126 and the *EGFL7* short transcript was significantly suppressed in H1975 and Calu-1 (Figs. 2*b*–2*d*). The 5-aza-CdR treatment of H1975 and Calu-1 restored the expression of mir-126 and the *EGFL7* short transcript (Figs. 2*b* and 2*c*), but the long *EGFL7* transcript (primer set 1 or 3) was not detected even after the 5-aza-CdR treatment of these two cell lines.

The 5′ CpG island of the *EGFL7* short transcript was heavily methylated in H1975 and Calu-1 but not in NHBE (Fig. 2*e*). To analyze the relation of the CpG island methylation status and miRNA expression, we performed a combined bisulfite restriction analysis (COBRA)[24] of the two CpG islands (CpG island 1 and CpG island 2, shown in Fig. 2*a*).

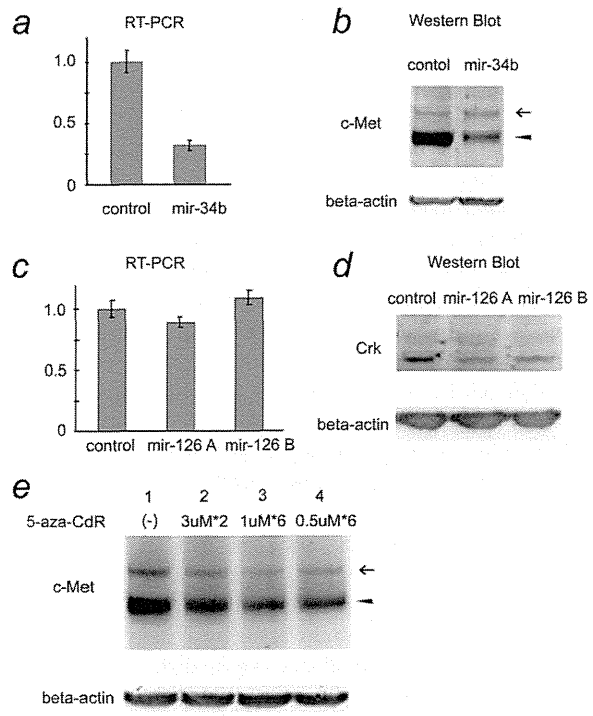

Figure 4. Analysis of miRNA targets. (*a*) RT-PCR of c-Met after the introduction of mir-34b into A549 cells. The vertical axis indicates the relative expression compared to that of the control vector. Experiments were duplicated, and the error bars indicate the SD. (*b*) Western blot of c-Met after the introduction of mir-34b into A549 cells. Both the c-Met precursor (arrow) and the c-Met beta subunit (arrowhead) are visible. (*c*) RT-PCR of Crk after the introduction of mir-126 into HEK293t cells. The vertical axis indicates the relative expression compared to that of the control vector. Experiments were triplicated, and the error bars indicate the SD. (*d*) Western blot of Crk after the introduction of mir-126 into HEK293t cells. Both mir-126A and mir-126B are miRNA expression vectors, but they have hygromycin resistance cassettes in different directions (Refer to Supporting Information Fig. 1). (*e*) Reduced c-Met protein after 5-aza-CdR treatment in H2347 cells. H2347 cells were treated with various concentrations of 5-aza-CdR (Lane 1, no treatment; Lane 2, 3 μM for 24 hr on Day 1 and Day 3, total protein was isolated on Day 6; Lane 3, 1 μM for six consecutive days, medium was changed every day, total protein was isolated on Day 7 and Lane 4, 0.5 μM for six consecutive days, medium was changed every day, total protein was isolated on Day 7). Both the c-Met precursor (arrow) and the c-Met beta subunit (arrowhead) are visible, similar to Figure 4*b*.

The DNA methylation of CpG island 1 was associated with a decrease in mir-126 expression. In contrast, the DNA methylation of CpG island 2 was not related to the expression of mir-126 (Fig. 2*f*). These results show that mir-126 is epigenetically silenced by the DNA methylation of its host gene, *EGFL7*.

We also analyzed the expression of intronic miRNAs and their host genes for the four remaining candidate miRNAs (mir-30e, mir-449a, mir-486 and mir-139; Supporting Information Fig. 4). The expressions of mir-139 and mir-449a were correlated with the expressions of their host genes, PED2A and CDC20B, respectively. However, the CpG islands of these host genes had only a low level of methylation in our NSCLC cell lines (data not shown).

Chromatin immunoprecipitation assay

To further analyze the regulation of miRNA expression, we examined the histone modifications of mir-34b and mir-126 using a ChIP assay. We observed the enrichment of H3K4me3 in the 5′ region of mir-34b in NHBE, but not in LC1sq (Fig. 3*a*). The H3K4me3 peak was restored in LC1sq after 5-aza-CdR treatment (Fig. 3*a*). Mir-34b was enriched with H3K9 methylation (H3K9me2 and H3K9me3) in LC1sq and, contrary to our expectations, also in NHBE (Supporting Information Fig. 5*b*). Although we cannot rule out the possibility of the nonspecific binding of the H3K9me2 and H3K9me3 antibodies, H3K9 methylation can occur without DNA methylation.[25] In fact, the relative mir-34b expression level in NHBE, compared to that in normal lung tissue, was 0.11 (0.10–0.13, mean ± SD), and the H3K9 methylation of NHBE may explain this suppression.

For the analysis of mir-126, we used two cell lines without CpG island methylation (NHBE and LC1sq) and two cell lines with heavily methylated CpG islands (H1975 and Calu-1). We detected the H3K4me3 peak in NHBE and LC1sq (Fig. 3*b*). This peak was very small in H1975 and Calu-1 and was induced after 5-aza-CdR treatment in both cell lines (Fig. 3*b*). The location of the H3K4me3 peak (primer 4, shown in Fig. 3*b*) was the same as the region of DNA methylation observed in H1975 and Calu-1 (shown in Fig. 2*e*). These results indicate that the DNA methylation near the transcriptional start site regulates *EGFL7* and mir-126 expression.

Unlike mir-34b, the *EGFL7* locus was enriched not only with H3K9 methylation but also with H3K27me3 (Supporting Information Fig. 5*c*). H3K27me3 was especially enriched in H1975, suggesting that both DNA methylation and H3K27me3 contribute to the epigenetic silencing of mir-126.

Target gene analysis of mir-34b and mir-126

To identify the target genes of mir-34b and mir-126, we used a database for the prediction of miRNA targets (Target Scan Human, http://targetscan.org).[26] Among the numerous predicted targets of mir-34b, we selected c-Met because c-Met has an oncogenic function in many human malignancies.[27] The overexpression of mir-34b using a U6 promoter-based expression vector[21] in A549 resulted in the decreased expression of c-Met at both the mRNA and protein levels (Figs. 4*a* and 4*b*). Mir-34b was completely methylated in H2347 (Figs. 1*b* and 1*c*), and the treatment of this cell line with 5-aza-CdR decreased the c-Met protein level (Fig. 4*e*).

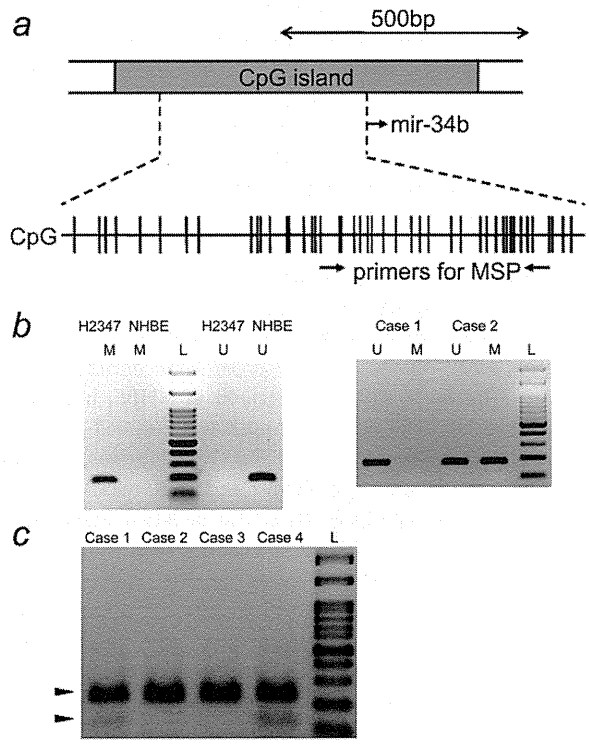

Figure 5. Methylation analysis of clinical tumor samples. Structure of mir-34b locus. (*a*) The CpG sites and the locations of the MSP primers are shown. (*b*) MSP analysis of mir-34b. H2347 and NHBE were used for the methylated and unmethylated controls. The bands in the "M" lanes are PCR products obtained using methylation-specific primers. The bands in the "U" lanes are PCR products obtained using unmethylated-specific primers. Mir-34b was methylated in case 2 but not in case 1. (*c*) COBRA of mir-126. Arrowheads indicate undigested and digested DNA fragments. Mir-126 was methylated in cases 1 and 4 (L, 100-bp DNA ladder).

We selected Crk as the target of mir-126 because an increase in Crk expression is associated with an aggressive phenotype in lung adenocarcinoma.[28] In agreement with previous reports[29,30] the overexpression of mir-126 in HEK293t decreased the Crk protein level without a significant change in the mRNA level (Figs. 4*c* and 4*d*).

DNA methylation analysis of primary NSCLCs and pathological characteristics

We analyzed the DNA methylation status of the two miRNAs in 99 primary NSCLCs, including 80 cases of adenocarcinoma, 18 cases of squamous cell carcinoma and 1 case of both histological components. There were 41 cases with T1 disease (<30 mm in diameter) without lymph node metastasis, 14 cases with T1 disease with lymph node metastasis, 27 cases with T2 disease (more than 30 mm in diameter or pleural invasion) without lymph node metastasis and 17 cases with T2 disease with lymph node metastasis. The DNA methylation status of mir-34b was determined using MSP[31] (Figs. 5*a* and 5*b*). For mir-126, the DNA methylation status of the 5′ CpG island of *EGFL7* was determined using COBRA (Fig. 5*c*; same protocol as that used for COBRA of CpG island 1, shown in Figs. 2*e* and 2*f*). We attempted to design MSP primers for the methylation analysis of mir-126, but the region of DNA methylation was less than 100 bp (Fig. 2*e*), and we could not design appropriate primers in this region. PCR amplification was successful in 96 samples.

Mir-34b and mir-126 were methylated in 40 (41%) and 7 (7%) of 96 the samples, respectively. To analyze the impact of miRNA methylation on the expression of a target oncogene, we performed immunohistochemistry for c-Met in 89 cases (Supporting Information Fig. 6). However, no correlation was observed between the miRNA methylation status and the c-Met expression level [(b) in Table 1], meaning that other mechanisms, such as gene amplification, are important for determining the c-Met expression level.

In a univariate analysis, both mir-34b methylation (chi-square test, $p = 0.016$) and c-Met expression (Fisher's exact test, $p = 0.026$) were associated with lymphatic invasion [(b and c) in Table 1]. In a multivariate analysis (stepwise logistic regression analysis), both mir-34b methylation ($p = 0.007$, odds ratio = 5.4) and c-Met expression ($p = 0.005$, odds ratio = 6.4) were associated with lymphatic invasion, whereas other clinical variables (age, gender, smoking, histology and tumor size) were not associated with lymphatic invasion [(d) in Table 1]. Therefore, both mir-34b methylation and c-Met expression were independent risk factors for lymphatic invasion.

The mir-126 methylation tended to be more frequent in tumors with venous invasion [(b) in Table 1], but the difference was not statistically significant (Fisher's exact test, $p = 0.084$). The mir-126 methylation was not associated with venous invasion in a multivariate analysis (data not shown).

Discussion

In our study, we analyzed 55 candidate miRNAs of which two were silenced by DNA methylation. The silencing mechanisms of the two miRNAs were different. Mir-34b was silenced by the DNA methylation of its own promoter, whereas mir-126 was silenced by the DNA methylation of its host gene's promoter.

Our initial *in silico* selected miRNAs included nine miRNAs within 1 kbp downstream of CpG islands, but none of these miRNAs were silenced by DNA methylation. This result may be partly because the primary miRNA transcripts are sometimes transcribed from more than 1 kb upstream of mature miRNAs, such as mir-21 and mir-155.[32,33] Further research is required for the epigenetic regulation of miRNAs, especially those located more than 1 kb downstream of CpG islands or those located within introns and coregulated with their host genes.

The mir-34 family consists of three miRNAs (mir-34a, mir-34b and mir-34c) that are derived from two transcripts

Table 1. MiRNA methylation and clinicopathological characteristics

(a) Clinical backgrounds of 96 cases in which PCR amplification was successful	
	Number of cases (*n*)
Age	≥65 years, $n = 51$; <65 years, $n = 45$
Gender	Male, $n = 59$; female, $n = 37$
Smoking	Smoker, $n = 63$; nonsmoker, $n = 33$
Histology	Adenocarcinoma, $n = 78$; squamous cell carcinoma, $n = 17$; adenosquamous carcinoma, $n = 1$
Tumor size	T1, $n = 53$; T2, $n = 43$

(b) Correlation of miRNA methylation and pathological characteristics				
		Methylated (*n*)	Unmethylated (*n*)	*p* Values
mir-34b methylation and lymphatic invasion	Invasion (–)	25	47	
	Invasion (+)	15	9	0.016[1]
mir-34b methylation and venous invasion	Invasion (–)	22	36	
	Invasion (+)	18	20	0.35[1]
mir-126 methylation and lymphatic invasion	Invasion (–)	4	68	
	Invasion (+)	3	21	0.23[2]
mir-126 methylation and venous invasion	Invasion (–)	2	56	
	Invasion (+)	5	33	0.084[2]
mir-34b methylation and c-Met expression	c-Met (–)	31	39	
	c-Met (+)	5	14	0.15[1]

(c) Correlation of clinicopathological characteristics and lymphatic invasion				
	Invasions	Number of cases (*n*)		*p* Values
Age	(–)	≥65 years, $n = 36$	<65 years, $n = 36$	
	(+)	≥65 years, $n = 15$	<65 years, $n = 9$	0.28[1]
Gender	(–)	Male, $n = 44$	Female, $n = 28$	
	(+)	Male, $n = 15$	Female, $n = 9$	0.90[1]
Smoking	(–)	Smoker, $n = 47$	Nonsmoker, $n = 25$	
	(+)	Smoker, $n = 16$	Nonsmoker, $n = 8$	0.90[1]
Histology	(–)	Adenocarcinoma, $n = 59$	Squamous cell carcinoma, $n = 13$	
	(+)	Adenocarcinoma, $n = 19$	Squamous cell carcinoma, $n = 4$	0.60[2]
Tumor size	(–)	T1, $n = 41$	T2, $n = 31$	
	(+)	T1, $n = 12$	T2, $n = 12$	0.55[1]
c-Met expression	(–)	c-Met (+), $n = 11$	c-Met (–), $n = 58$	
	(+)	c-Met (+), $n = 8$	c-Met (–), $n = 12$	0.026[2]

(d) Stepwise logistic regression analysis for risk factors of lymphatic invasion		
	Odds ratio (95 % confidential interval)	*p* Values
mir-34b methylation (methylated or unmethylated)	5.494 (1.585–19.047)	0.007
c-Met expression (positive or negative)	6.492 (1.738–24.256)	0.005

[1]Chi-square test. [2]Fisher's exact test.

(mir-34a on chromosome 1 and mir-34b/c on chromosome 11). Mir-34s have been shown to be direct targets of p53.[34–36] Interestingly, mir-34a is most highly expressed in the brain, whereas mir-34b/c is most highly expressed in the lung with a low expression in the brain and no expression in any other tissues,[36] suggesting that mir-34b/c plays an important role in the p53 tumor suppressive pathway, at least in lung tissue.

In our study, we showed the importance of DNA methylation in the regulation of mir-34b expression in lung cancer and the suppression of the c-Met oncogene by its overexpression. Among the numerous predicted targets of mir-34b, we selected c-Met for further analysis, because it is an important target of cancer therapy,[37] and its amplification has been reported to be a mechanism of acquired resistance to gefitinib therapy in NSCLC.[38] We observed increased mir-34b

expression and reduced c-Met protein after 5-aza-CdR treatment of H2347 cells. This does not necessarily mean that mir-34b reexpression was responsible for c-Met reduction, as 5-aza-CdR treatment induces many silenced genes. A recent study showed that treatment of the colon cancer cell line HCT116 with 5-aza-CdR induced an abnormal fusion transcript of LINE-1 and c-Met that did not code for a normal c-Met protein.[39] Further research is required to understand the molecular basis of epigenetic drug actions.

We also observed a strong association between mir-34b methylation and lymphatic invasion in clinical tumor samples, in agreement with a previous report that mir-34b methylation is correlated with metastasis in human cancers.[10] Migliore *et al.*[40] reported that mir-34s suppress c-Met and impair invasion in several cancer cell lines. In their study, c-Met overexpression rescued impaired cell invasion, and therefore, they concluded that mir-34s suppress invasion through the downregulation of c-Met *in vitro*. However, in our study, mir-34b methylation and c-Met expression were independent, and both of them were associated with lymphatic invasion. Our results suggest that the regulation of c-Met expression and tumor invasion is more complex *in vivo*. Although the pathological phenotype associated with mir-34b methylation was similar to that associated with c-Met overexpression, the loss of mir-34b probably does not induce c-Met overexpression directly in primary NSCLCs.

Mir-126 is a tumor suppressive miRNA, suppressing metastasis in breast cancer[41] and inhibiting invasion by targeting Crk in NSCLC.[29] Using bladder cancer cell lines, Saito reported that epigenetic therapy upregulates mir-126 and its host gene *EGFL7*, but DNA methylation was not detected in the *EGFL7* promoter region.[42] Here, we showed that mir-126 is silenced by the DNA methylation of its host gene, *EGFL7* in lung cancer. Many miRNAs are located within introns of protein coding genes, and intronic miRNAs are usually coordinately expressed with their host gene mRNAs.[43] Grady reported that mir-342 is epigenetically silenced by the DNA methylation of its host gene, Enah/Vasp-like (EVL) in colorectal cancer[44]; thus, mir-126 is the second miRNA silenced by the DNA methylation of its host gene.

We also showed that the *EGFL7* locus was enriched with H3K27me3, which is consistent with a previous report that polycomb-mediated H3K27me3 premarks genes for *de novo* DNA methylation in colon cancer.[20] In contrast, Kondo reported that H3K27me3 mediates gene silencing independent of DNA methylation in prostate cancer.[45] Although mir-126 expression was frequently suppressed in clinical tumor samples, the frequency and the degree of DNA methylation were low in our analysis using COBRA, and this discrepancy may be explained by H3K27me3.

In conclusion, genome structure-based screening was used to identify two epigenetically silenced tumor suppressive miRNAs. Our genome-structure based approach can be applied to identify epigenetically silenced miRNAs in other malignancies. The DNA methylation of mir-34b can be used as a biomarker for an invasive phenotype of lung cancer.

References

1. Bartel DP. MicroRNAs: genomics, biogenesis, mechanism, and function. *Cell* 2004;116:281–97.
2. Calin GA, Dumitru CD, Shimizu M, Bichi R, Zupo S, Noch E, Aldler H, Rattan S, Keating M, Rai K, Rassenti L, Kipps T, et al. Frequent deletions and down-regulation of micro- RNA genes miR15 and miR16 at 13q14 in chronic lymphocytic leukemia. *Proc Natl Acad Sci USA* 2002;99:15524–9.
3. Takamizawa J, Konishi H, Yanagisawa K, Tomida S, Osada H, Endoh H, Harano T, Yatabe Y, Nagino M, Nimura Y, Mitsudomi T, Takahashi T. Reduced expression of the let-7 microRNAs in human lung cancers in association with shortened postoperative survival. *Cancer Res* 2004;64:3753–6.
4. Hayashita Y, Osada H, Tatematsu Y, Yamada H, Yanagisawa K, Tomida S, Yatabe Y, Kawahara K, Sekido Y, Takahashi T. A polycistronic microRNA cluster, miR-17–92, is overexpressed in human lung cancers and enhances cell proliferation. *Cancer Res* 2005;65:9628–32.
5. Yanaihara N, Caplen N, Bowman E, Seike M, Kumamoto K, Yi M, Stephens RM, Okamoto A, Yokota J, Tanaka T, Calin GA, Liu CG, et al. Unique microRNA molecular profiles in lung cancer diagnosis and prognosis. *Cancer Cell* 2006;9: 189–98.
6. He L, Thomson JM, Hemann MT, Hernando-Monge E, Mu D, Goodson S, Powers S, Cordon-Cardo C, Lowe SW, Hannon GJ, Hammond SM. A microRNA polycistron as a potential human oncogene. *Nature* 2005;435:828–33.
7. Jones PA, Baylin SB. The fundamental role of epigenetic events in cancer. *Nat Rev Genet* 2002;3:415–28.
8. Herman JG, Baylin SB. Gene silencing in cancer in association with promoter hypermethylation. *N Engl J Med* 2003;349: 2042–54.
9. Saito Y, Liang G, Egger G, Friedman JM, Chuang JC, Coetzee GA, Jones PA. Specific activation of microRNA-127 with downregulation of the proto-oncogene BCL6 by chromatin-modifying drugs in human cancer cells. *Cancer Cell* 2006;9: 435–43.
10. Lujambio A, Calin GA, Villanueva A, Ropero S, Sanchez-Cespedes M, Blanco D, Montuenga LM, Rossi S, Nicoloso MS, Faller WJ, Gallagher WM, Eccles SA, et al. A microRNA DNA methylation signature for human cancer metastasis. *Proc Natl Acad Sci USA* 2008;105:13556–61.
11. Sano A, Kage H, Sugimoto K, Kitagawa H, Aki N, Goto A, Fukayama M, Nakajima J, Takamoto S, Nagase T, Yatomi Y, Ohishi N, et al. A second-generation profiling system for quantitative methylation analysis of multiple gene promoters: application to lung cancer. *Oncogene* 2007; 26:6518–25.
12. Kusakabe M, Kutomi T, Watanabe K, Emoto N, Aki N, Kage H, Hamano E, Kitagawa H, Nagase T, Sano A, Yoshida Y, Fukami T, et al. Identification of G0S2 as a gene frequently methylated in squamous lung cancer by combination of in silico and experimental approaches. *Int J Cancer* 2010;126:1895–902.
13. Brock MV, Hooker CM, Ota-Machida E, Han Y, Guo M, Ames S, Glockner S, Piantadosi S, Gabrielson E, Pridham G, Pelosky K, Belinsky SA, et al. DNA methylation markers and early recurrence in stage I lung cancer. *N Engl J Med* 2008; 358:1118–28.
14. Takai D, Yagi Y, Wakazono K, Ohishi N, Morita Y, Sugimura T, Ushijima T. Silencing of HTR1B and reduced expression of EDN1 in human lung

cancers, revealed by methylation-sensitive representational difference analysis. *Oncogene* 2001;20:7505–13.
15. Sambrook J, Russell DW. Molecular Cloning 3rd Editioned., vol. 1, chapter 6. New York:CSHL Press, 2001.
16. Singer-Sam J, LeBon JM, Tanguay RL, Riggs AD. A quantitative HpaII-PCR assay to measure methylation of DNA from a small number of cells. *Nucleic Acids Res* 1990;18:687.
17. Watanabe K, Emoto N, Sunohara M, Kawakami M, Kage H, Nagase T, Ohishi N, Takai D. Treatment of PCR products with exonuclease I and heat-labile alkaline phosphatase improves the visibility of combined bisulfite restriction analysis. *Biochem Biophys Res Commun* 2010;399: 422–4.
18. Kusakabe M, Watanabe K, Emoto N, Aki N, Kage H, Nagase T, Nakajima J, Yatomi Y, Ohishi N, Takai D. Impact of DNA demethylation of the G0S2 gene on the transcription of G0S2 in squamous lung cancer cell lines with or without nuclear receptor agonists. *Biochem Biophys Res Commun* 2009;390:1283–7.
19. Cao R, Zhang Y. SUZ12 is required for both the histone methyltransferase activity and the silencing function of the EED-EZH2 complex. *Mol Cell* 2004;15: 57–67.
20. Schlesinger Y, Straussman R, Keshet I, Farkash S, Hecht M, Zimmerman J, Eden E, Yakhini Z, Ben-Shushan E, Reubinoff BE, Bergman Y, Simon I, et al. Polycomb-mediated methylation on Lys27 of histone H3 pre-marks genes for de novo methylation in cancer. *Nat Genet* 2007;39: 232–6.
21. Matsukura S, Jones PA, Takai D. Establishment of conditional vectors for hairpin siRNA knockdowns. *Nucleic Acids Res* 2003;31:e77.
22. Nakamura Y, Niki T, Goto A, Morikawa T, Miyazawa K, Nakajima J, Fukayama M. c-Met activation in lung adenocarcinoma tissues: an immunohistochemical analysis. *Cancer Sci* 2007;98:1006–13.
23. Toyota M, Suzuki H, Sasaki Y, Maruyama R, Imai K, Shinomura Y, Tokino T. Epigenetic silencing of microRNA-34b/c and B-cell translocation gene 4 is associated with CpG island methylation in colorectal cancer. *Cancer Res* 2008;68: 4123–32.
24. Xiong Z, Laird PW. COBRA: a sensitive and quantitative DNA methylation assay. *Nucleic Acids Res* 1997;25:2532–4.
25. Bachman KE, Park BH, Rhee I, Rajagopalan H, Herman JG, Baylin SB, Kinzler KW, Vogelstein B. Histone modifications and silencing prior to DNA methylation of a tumor suppressor gene. *Cancer Cell* 2003;3:89–95.
26. Grimson A, Farh KK, Johnston WK, Garrett-Engele P, Lim LP, Bartel DP. MicroRNA targeting specificity in mammals: determinants beyond seed pairing. *Mol Cell* 2007;27:91–105.
27. Peruzzi B, Bottaro DP. Targeting the c-Met signaling pathway in cancer. *Clin Cancer Res* 2006;12:3657–60.
28. Miller CT, Chen G, Gharib TG, Wang H, Thomas DG, Misek DE, Giordano TJ, Yee J, Orringer MB, Hanash SM, Beer DG. Increased C-CRK proto-oncogene expression is associated with an aggressive phenotype in lung adenocarcinomas. *Oncogene* 2003;22:7950–7.
29. Crawford M, Brawner E, Batte K, Yu L, Hunter MG, Otterson GA, Nuovo G, Marsh CB, Nana-Sinkam SP. MicroRNA-126 inhibits invasion in non-small cell lung carcinoma cell lines. *Biochem Biophys Res Commun* 2008;373:607–12.
30. Li X, Shen Y, Ichikawa H, Antes T, Goldberg GS. Regulation of miRNA expression by Src and contact normalization: effects on nonanchored cell growth and migration. *Oncogene* 2009;28: 4272–83.
31. Herman JG, Graff JR, Myohanen S, Nelkin BD, Baylin SB. Methylation-specific PCR: a novel PCR assay for methylation status of CpG islands. *Proc Natl Acad Sci USA* 1996; 93:9821–6.
32. Cai X, Hagedorn CH, Cullen BR. Human microRNAs are processed from capped, polyadenylated transcripts that can also function as mRNAs. *RNA* 2004;10:1957–66.
33. Eis PS, Tam W, Sun L, Chadburn A, Li Z, Gomez MF, Lund E, Dahlberg JE. Accumulation of miR-155 and BIC RNA in human B cell lymphomas. *Proc Natl Acad Sci USA* 2005;102:3627–32.
34. Corney DC, Flesken-Nikitin A, Godwin AK, Wang W, Nikitin AY. MicroRNA-34b and MicroRNA-34c are targets of p53 and cooperate in control of cell proliferation and adhesion-independent growth. *Cancer Res* 2007;67:8433–8.
35. He L, He X, Lim LP, de Stanchina E, Xuan Z, Liang Y, Xue W, Zender L, Magnus J, Ridzon D, Jackson AL, Linsley PS, et al. A microRNA component of the p53 tumour suppressor network. *Nature* 2007;447: 1130–4.
36. Bommer GT, Gerin I, Feng Y, Kaczorowski AJ, Kuick R, Love RE, Zhai Y, Giordano TJ, Qin ZS, Moore BB, MacDougald OA, Cho KR, et al. p53-mediated activation of miRNA34 candidate tumor-suppressor genes. *Curr Biol* 2007;17:1298–307.
37. Eder JP, Vande Woude GF, Boerner SA, LoRusso PM. Novel therapeutic inhibitors of the c-Met signaling pathway in cancer. *Clin Cancer Res* 2009;15:2207–14.
38. Engelman JA, Zejnullahu K, Mitsudomi T, Song Y, Hyland C, Park JO, Lindeman N, Gale CM, Zhao X, Christensen J, Kosaka T, Holmes AJ, et al. MET amplification leads to gefitinib resistance in lung cancer by activating ERBB3 signaling. *Science* 2007;316:1039–43.
39. Weber B, Kimhi S, Howard G, Eden A, Lyko F. Demethylation of a LINE-1 antisense promoter in the cMet locus impairs Met signalling through induction of illegitimate transcription. *Oncogene* 2010;29:5775–84.
40. Migliore C, Petrelli A, Ghiso E, Corso S, Capparuccia L, Eramo A, Comoglio PM, Giordano S. MicroRNAs impair MET-mediated invasive growth. *Cancer Res* 2008;68:10128–36.
41. Tavazoie SF, Alarcon C, Oskarsson T, Padua D, Wang Q, Bos PD, Gerald WL, Massague J. Endogenous human microRNAs that suppress breast cancer metastasis. *Nature* 2008;451:147–52.
42. Saito Y, Friedman JM, Chihara Y, Egger G, Chuang JC, Liang G. Epigenetic therapy upregulates the tumor suppressor microRNA-126 and its host gene EGFL7 in human cancer cells. *Biochem Biophys Res Commun* 2009;379:726–31.
43. Baskerville S, Bartel DP. Microarray profiling of microRNAs reveals frequent coexpression with neighboring miRNAs and host genes. *RNA* 2005;11: 241–7.
44. Grady WM, Parkin RK, Mitchell PS, Lee JH, Kim YH, Tsuchiya KD, Washington MK, Paraskeva C, Willson JK, Kaz AM, Kroh EM, Allen A, et al. Epigenetic silencing of the intronic microRNA hsa-miR-342 and its host gene EVL in colorectal cancer. *Oncogene* 2008;27: 3880–8.
45. Kondo Y, Shen L, Cheng AS, Ahmed S, Boumber Y, Charo C, Yamochi T, Urano T, Furukawa K, Kwabi-Addo B, Gold DL, Sekido Y, et al. Gene silencing in cancer by histone H3 lysine 27 trimethylation independent of promoter DNA methylation. *Nat Genet* 2008;40:741–50.

Pulmonary Venous Invasion, Determined by Chest Computed Tomographic Scan, as a Potential Early Indicator of Zygomycosis Infection

A Case Series

Hiroshi Kitagawa, MD, PhD, Kousuke Watanabe, MD,* Hidenori Kage, MD, PhD,* Shinichi Inoh, MD,† Akiteru Goto, MD, PhD,‡ Masashi Fukayama, MD, PhD,‡ Takahide Nagase, MD, PhD,* Nobuya Ohishi, MD, PhD,* and Daiya Takai, MD, PhD§*

Abstract: Zygomycosis is a life-threatening fungal infection, and its successful treatment requires early diagnosis. To establish radiologic and clinical criteria for early diagnosis, we reviewed 3 postmortem cases with zygomycosis secondary to hematological diseases. In all cases, an irregular dilatation of pulmonary veins on computed tomography suggested venous invasion by fungal hyphae, which was confirmed at autopsy. In addition, serum samples tested negative for the Aspergillus galactomannan antigen in all cases. These distinguishing radiologic and clinical features may contribute to an earlier diagnosis; more radical treatments, such as amphotericin-B or pulmonary resection; and a more successful outcome for patients with zygomycosis.

Key Words: zygomycosis, fungal infection, pulmonary vein, hematological disease, computed tomography

(*J Thorac Imaging* 2012;27:W97–W99)

Zygomycosis is caused by the members of the class *Zygomycetes*, including *Mucorales* and *Entomophthorales*, and is known as an invasive infection that occurs in immunocompromised patients, such as those suffering from hematological disorders.[1,2] Recent increased treatment of hematological diseases with chemotherapy coupled with the use of azole antifungal agents for prevention of deep mycosis, such as candidiasis and aspergillosis, has led to the development of zygomycosis with considerable intrinsic resistance to this prophylaxis.[3] Due to this organism's strong ability to invade blood vessels, multiple organs are often involved, and dissemination may occur in affected patients.[1] Pulmonary involvement is seen in approximately 60% of patients and is associated with mortality rates as high as 76%.[4]

Although clinical factors such as underlying diseases, iron overload, and prophylactic use of azole antifungal agents may predispose a patient to zygomycosis, the early diagnosis of this infection is still difficult. It is especially challenging to differentiate it from invasive aspergillosis. Computed tomography (CT) is a powerful tool for the diagnosis of fungal infections.[5] The reported CT manifestations of pulmonary zygomycosis include cavity formation, consolidation, pleural effusion, and pulmonary artery pseudoaneurysm in the advanced stage.[5,6] However, to our knowledge, there is a paucity of literature that describes the radiologic findings of pulmonary zygomycosis with autopsy confirmation. In addition, pulmonary venous invasion, as seen on chest CT, has not been reported as a criterion for the early diagnosis of zygomycosis. From our autopsy files collected over a 4-year period of patients with hematological disease and pulmonary lesions, we reviewed 3 cases with zygomycotic infection to assess for characteristic CT and clinical findings to aid earlier diagnosis.

CASE REPORTS

Case 1

A 61-year-old man with diabetes mellitus and pre-B-cell-type acute lymphoblastic leukemia had a high-grade fever of 38.5°C at admission, and chest x-ray showed parenchymal air space opacity in the left upper lung area. Unenhanced CT scan showed well-defined ground-glass opacity with irregular pulmonary vein dilation in comparison with a previous CT (Figs. 1A, B). His white blood cell (WBC) count was 16800/mm^3, with 74% of blastocytes, and serum *Aspergillus* galactomannan antigen was negative. Despite treatment for 2 weeks with fluconazole and chemotherapy, hemorrhagic brain infarction developed and led to his death. Autopsy confirmed hemorrhagic pulmonary zygomycosis, with fungal hyphae in the pulmonary veins but not in the arteries (Figs. 1C, 2). Cerebral zygomycosis was also found.

Case 2

A 35-year-old man, who had been diagnosed with aplastic anemia at 14 years of age, presented with persistent pancytopenia. Chemotherapy was not effective, and blood transfusions were repeated. After preparative treatment with deferoxamine and fluconazole for hematopoietic stem cell transplantation, high-grade fever of 38.5°C and parenchymal air space opacity in the right upper to middle lung area on chest x-ray appeared. CT scans showed irregular pulmonary vein dilation and bronchial wall thickening surrounded by ground-glass opacity in the right middle lobe compared with previous CT (Fig. 3). His WBC count was 600/mm^3, and serum *Aspergillus* galactomannan antigen was negative. Even after 3 weeks of voriconazole and 1 week of amphotericin-B, respiratory failure progressed and led to his death. Autopsy showed

From the Departments of *Respiratory Medicine; †Clinical Laboratory; ‡Radiology; and §Pathology, Tokyo University Hospital, Bunkyo-ku, Tokyo, Japan.

This manuscript has been read and approved by all authors, who accept full responsibility for its content. All authors had full access to the data and their analysis and participated in the drafting and editing of the article. The authors also declare no conflict of interests regarding the study.

Supported by a research grant from St Luke's Life Science Institute.

Reprints: Hiroshi Kitagawa, MD, PhD, Department of Respiratory Medicine, Tokyo University Hospital, 7-3-1 Hongo, Bunkyo-ku, Tokyo, Japan 113-8655 (e-mail: hkitagawa-tky@umin.ac.jp).

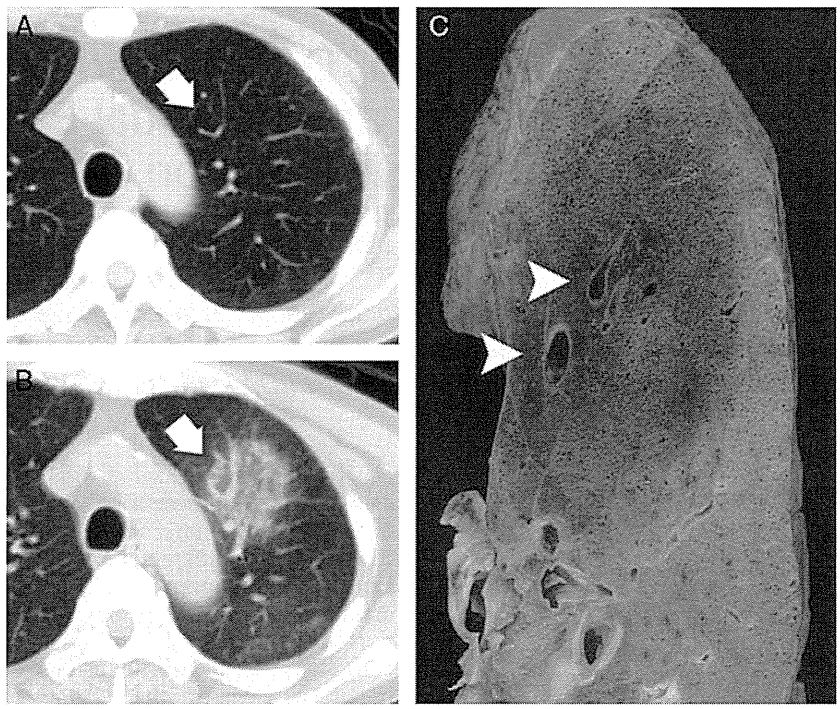

FIGURE 1. Irregular pulmonary vein dilation (case 1). A, Chest CT scan taken 8 months before the last admission shows normal pulmonary veins (arrow) in the upper lobe of the left lung. B, Chest CT scan taken during the last admission shows irregular pulmonary vein dilation (arrow) surrounded by ground-glass opacity. C, Pulmonary venous invasion is surrounded by hemorrhage at autopsy (arrowheads).

fungal hyphae invading the pulmonary veins and arteries, which resulted in hemorrhagic infarction of the lung.

Case 3

A 64-year-old man with overt leukemia from myelodysplastic syndrome developed a high-grade fever above 38°C, and his chest x-ray and chest CT scan revealed small nodules in the lungs bilaterally. His WBC count was 900/mm^3, and 36% of blastocytes was revealed. Serum *Aspergillus* galactomannan antigen was negative. After a 2-week course of voriconazole, a follow-up CT scan showed an increasing number of small nodules along with irregular dilation of the pulmonary veins in the right lung, compared with the CT at admission (Fig. 4). Despite treatment with amphotericin-B, right maxillary sinusitis developed, and progressive respiratory failure caused his death. At autopsy, fungal hyphae were found to have invaded the pulmonary vessels and bronchi, which resulted in massive hemorrhagic pulmonary infarction.

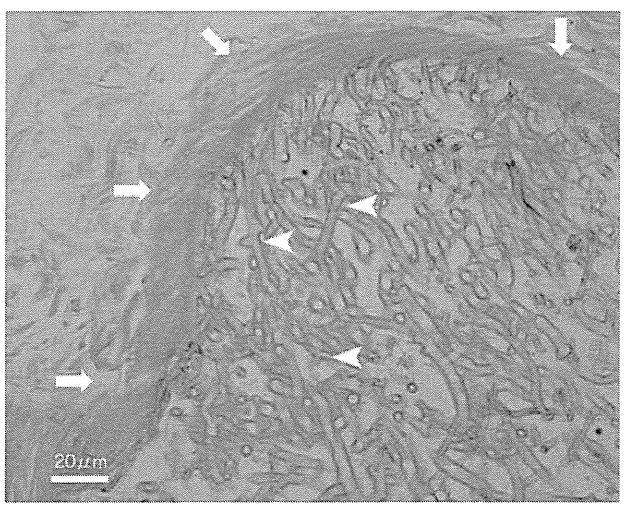

FIGURE 2. Spreading broad aseptate fungal hyphae in the pulmonary vein at autopsy of case 1 (Grocott's Methenamine Silver stain, ×400). The pulmonary vein and typical right-angle branching of the hyphae are indicated by arrows and arrowheads, respectively.

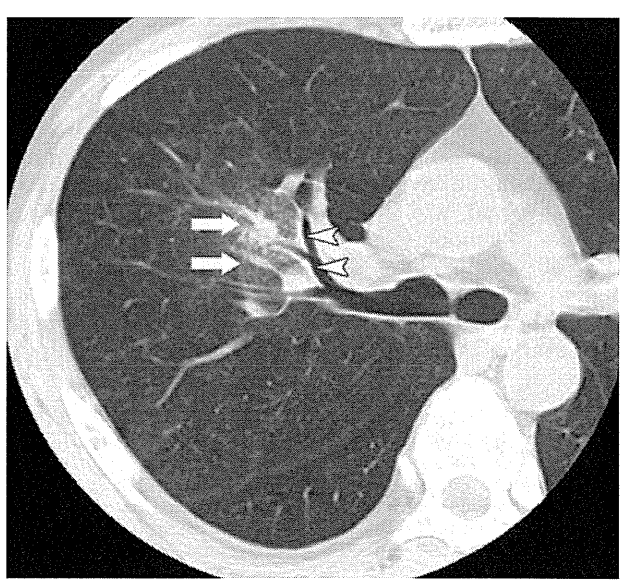

FIGURE 3. Irregular pulmonary vein dilation (case 2): chest CT scan taken during the last admission shows bronchial wall thickening (arrowhead) and irregular pulmonary vein dilation (arrows) surrounded by ground-glass opacity.

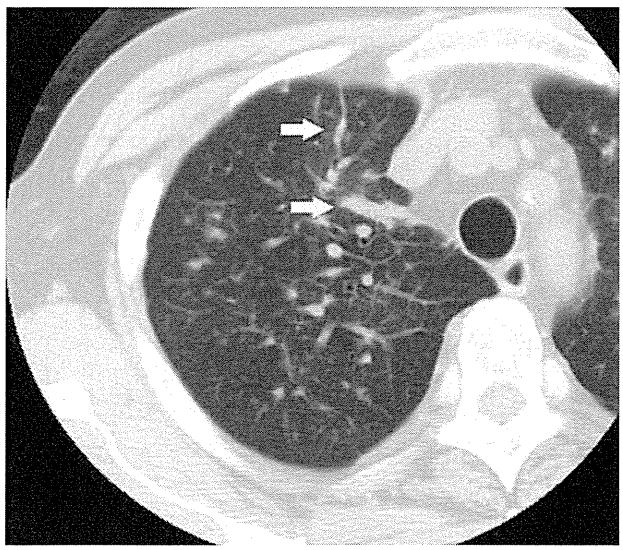

FIGURE 4. Irregular pulmonary vein dilation (case 3): chest CT scan taken 2 weeks after the last admission shows irregular pulmonary vein dilation (arrows) and increasing small nodules.

DISCUSSION

Although zygomycosis is the third most prevalent cause of fungal infection after aspergillosis and candidiasis, it is important to consider zygomycotic infection in patients with immunocompromised status or hematological disorders because of its high mortality rate.[2] Invasive aspergillosis is the most important differential diagnosis of zygomycosis. Radiologically, pleural effusion and pulmonary artery pseudoaneurysm are characteristic features of zygomycosis and are useful to distinguish between the 2 diseases[3,6]; however, these findings are thought to emerge in the advanced stages of disease and to be rare.[6] In the cases reviewed here, chest CT scans showed irregular dilation of the pulmonary veins, which proved the invasion by fungal hyphae on autopsy. As these changes preceded the hemorrhagic brain infarction (case 1), pleural effusion, and consolidation (cases 2 and 3), they can be regarded as earlier and more frequent indicators of zygomycosis. There may be several reasons why the development of venous invasion occurs in the earlier stages of zygomycosis. First, the pulmonary vein does not have a thick elastic layer compared with the pulmonary artery. Second, as the venous blood is better oxygenized than the arterial blood in the lung, the fungi may be able to invade easily and grow fast in the pulmonary veins. Thus, it is reasonable that the pulmonary venous finding may help to make an earlier decision for invasive diagnostic procedures or immediate treatment.

Circulating levels of galactomannan *Aspergillus* antigen are known to be a useful tool for the distinction between zygomycosis and invasive aspergillosis. When the test result is negative, it is highly unlikely that the diagnosis is invasive aspergillosis.[7] We observed a negative result for serum galactomannan *Aspergillus* antigen, and also decreased neutrophils and use of azole antifungal agents along with sinusitis or deferoxamine intake. This evidence strengthens the conclusion that combining the negative *Aspergillus* antigen result with other clinical information may be beneficial for the diagnosis of zygomycosis. Early diagnosis based on these characteristic findings can contribute to curative operation, adequate antifungal medication,[8] and the determination of involvement of other organs.[4] However, because this study included only 3 cases of zygomycosis, analyses of more cases are needed to verify these radiologic and clinical findings.

In summary, we report 3 cases of pulmonary zygomycosis occurring in patients with hematological diseases. Irregular pulmonary venous dilation on chest CT corresponds with autopsy findings of fungal angioinvasion. In addition to recognition of these characteristic CT findings, assessment of characteristic clinical risk factors may be useful for physicians to suspect the possibility of zygomycosis in order to contribute to earlier diagnosis, more successful treatment, and better clinical outcome.

ACKNOWLEDGMENT

The authors thank the NIH Fellows Editorial Board for reviewing the manuscript.

REFERENCES

1. Pagano L, Ricci P, Tonso A, et al. Mucormycosis in patients with haematological malignancies: a retrospective clinical study of 37 cases. *Br J Haematol.* 1997;99:331–336.
2. Chayakulkeeree M, Ghannoum MA, Perfect JR. Zygomycosis: the re-emerging fungal infection. *Eur J Clin Microbiol Infect Dis.* 2006;25:215–229.
3. Chamilos G, Marom EM, Lewis RE, et al. Predictors of pulmonary zygomycosis versus invasive pulmonary aspergillosis in patients with cancer. *Clinical Infectious Diseases.* 2005;41:60–66.
4. Roden MM, Zaoutis TE, Buchanan WL, et al. Epidemiology and outcome of zygomycosis: a review of 929 reported cases. *Clin Infect Dis.* 2005;41:634–653.
5. Won HJ, Lee KS, Cheon JE, et al. Invasive pulmonary aspergillosis: prediction at thin-section CT in patients with neutropenia—a prospective study. *Radiology.* 1998;208:777–782.
6. McAdams HP, Rosado de Christenso M, Strollo DC, et al. Pulmonary mucormycosis: radiologic findings in 32 cases. *Am J Roentgenol.* 1997;168:1541–1548.
7. Maertens J, Verhaegen J, Lagrou K, et al. Screening for circulating galactomannan as a noninvasive diagnostic tool for invasive aspergillosis in prolonged neutropenic patients and stem cell transplantation recipients: a prospective validation. *Blood.* 2001;97:1604–1610.
8. Gonzalez CE, Couriel DR, Walsh TJ. Disseminated zygomycosis in a neutropenic patient: successful treatment with amphotericin B lipid complex and granulocyte colony-stimulating factor. *Clin Infect Dis.* 1997;24:192–196.

OPEN ACCESS Freely available online

PLoS one

Quantitative Analysis of Viral Load per Haploid Genome Revealed the Different Biological Features of Merkel Cell Polyomavirus Infection in Skin Tumor

Satoshi Ota[1,2], Shumpei Ishikawa[2]*, Yutaka Takazawa[2], Akiteru Goto[2], Takeshi Fujii[3], Ken-ichi Ohashi[3], Masashi Fukayama[2]

1 Department of Pathology, Chiba University Hospital, University of Chiba, Chuo, Chiba, Chiba, Japan, **2** Department of Pathology, Graduate School of Medicine, University of Tokyo, Bunkyo, Tokyo, Japan, **3** Department of Pathology, Toranomon Hospital, Minato, Tokyo, Japan

Abstract

Merkel cell polyomavirus (MCPyV) has recently been identified in Merkel cell carcinoma (MCC), an aggressive cancer that occurs in sun-exposed skin. Conventional technologies, such as polymerase chain reaction (PCR) and immunohistochemistry, have produced conflicting results for MCPyV infections in non-MCC tumors. Therefore, we performed quantitative analyses of the MCPyV copy number in various skin tumor tissues, including MCC (n = 9) and other sun exposure-related skin tumors (basal cell carcinoma [BCC, n = 45], actinic keratosis [AK, n = 52], Bowen's disease [n = 34], seborrheic keratosis [n = 5], primary cutaneous anaplastic large-cell lymphoma [n = 5], malignant melanoma [n = 5], and melanocytic nevus [n = 6]). In a conventional PCR analysis, MCPyV DNA was detected in MCC (9 cases; 100%), BCC (1 case; 2%), and AK (3 cases; 6%). We then used digital PCR technology to estimate the absolute viral copy number per haploid human genome in these tissues. The viral copy number per haploid genome was estimated to be around 1 in most MCC tissues, and there were marked differences between the MCC (0.119–42.8) and AK (0.02–0.07) groups. PCR-positive BCC tissue showed a similar viral load as MCC tissue (0.662). Immunohistochemistry with a monoclonal antibody against the MCPyV T antigen (CM2B4) demonstrated positive nuclear localization in most of the high-viral-load tumor groups (8 of 9 MCC and 1 BCC), but not in the low-viral-load or PCR-negative tumor groups. These results demonstrated that MCPyV infection is possibly involved in a minority of sun-exposed skin tumors, including BCC and AK, and that these tumors display different modes of infection.

Citation: Ota S, Ishikawa S, Takazawa Y, Goto A, Fujii T, et al. (2012) Quantitative Analysis of Viral Load per Haploid Genome Revealed the Different Biological Features of Merkel Cell Polyomavirus Infection in Skin Tumor. PLoS ONE 7(6): e39954. doi:10.1371/journal.pone.0039954

Editor: Amanda Ewart Toland, Ohio State University Medical Center, United States of America

Received January 10, 2012; **Accepted** May 29, 2012; **Published** June 29, 2012

Funding: This study was supported by the Industrial Technology Research Grant Program of the New Energy and Industrial Technology Development Organization (NEDO) of Japan (S.I.) and Grants-in-Aid for Scientific Research on Innovative Areas from the Ministry of Education, Culture, Sports, Science and Technology of Japan (S.I.). The funders had no role in study design, data collection and analysis, decision to publish, or preparation of the manuscript.

Competing Interests: The authors have declared that no competing interests exist.

* E-mail: isikawas-tky@umin.org

Introduction

Merkel cell carcinoma (MCC), which is a rare and aggressive primary cutaneous neoplasm that affects elderly and/or immunocompromised individuals, tends to occur in sun-exposed skin [1]. The Merkel cell polyomavirus (MCPyV) was recently identified in MCC [2], and its frequency in MCC has been reported to be 100% by immunohistochemical and/or polymerase chain reaction (PCR) studies that were performed in western countries [2–23] and in East Asia [24–27]. The monoclonal integration of MCPyV DNA in host DNA has been demonstrated in neoplastic MCC cells, indicating that the virus causes and/or promotes this specific type of cutaneous neoplasm [2]. However, it remains unclear how often MCPyV is associated with other cutaneous neoplasms and to what extent racial factors influence the infection rates. In skin tumors other than MCC, MCPyV has been detected at various frequencies (0%–25%) by PCR. However, immunohistochemical analyses have suggested that MCPyV is specific to MCC and is absent from other skin tumors, including squamous cell carcinoma, basal cell carcinoma (BCC), and lymphoma [28,29]. MCPyV T-antigen expression may be suppressed in infected cells in certain circumstances, even though MCPyV viral DNA is integrated into the cellular DNA. A significant number of MCPyV-positive cases are positive for the small-T (ST) antigen but do not express the large-T (LT) antigen [30]. Recently, Neumann et al. found that all integrated genomes had truncation mutations in the LT antigen [31]. However, it may be difficult to address these issues without a sensitive quantitative detection method.

In the present study, we investigated the frequency of MCPyV infection in skin tumors, including MCC and other sun exposure-related skin tumors, such as BCC, actinic keratosis (AK), and Bowen's disease (BD), in Japan. Other representative non-melanocytic, melanocytic, and lymphoid skin tumors were also included. We applied digital PCR in order to calculate the absolute viral copy number per haploid human genome [32,33]. This method uses nanofluidic technology to randomly distribute applied DNA molecules to multiple small reaction chambers at a concentration of 0 to 1 DNA molecules per chamber. Target and reference genes are simultaneously PCR-amplified with a dual-color amplification reaction, and their copy numbers are then calculated by counting the numbers of signal-positive chambers. This PCR-efficiency-independent method is highly robust for comparing copy numbers using different primer sets. The results